

Original paper

Mineralogical and geochemical studies of Cu–Bi–Ag±W ores from Janjevo (Kosovo): Insights into the Bi sulfosalt mineralogy and the distribution of bismuth in base metal sulfides

Sławomir MEDERSKI^{1*}, Jaroslav PRŠEK¹, Joanna KOŁODZIEJCZYK¹, Konrad KLUZA¹, Vasilios MELFOS², Katarzyna ADAMEK¹, Dimitrina DIMITROVA³

¹ Faculty of Geology, Geophysics and Environmental Protection, AGH UST, University of Science and Technology, 30 Mickiewicz Av., 30-059 Kraków, Poland; mederski@agh.edu.pl

² Department of Mineralogy, Petrology and Economic Geology, Faculty of Geology, Aristotle University of Thessaloniki, Thessaloniki 54124, Greece

³ Geological Institute, Bulgarian Academy of Sciences, 1113 Sofia, Bulgaria

*Corresponding author



This work presents a mineralogical and geochemical study of Cu–Bi–Ag±W ores from Janjevo in the Trepça Mineral Belt in Kosovo. This locality indicates a new type of Bi–Cu±Au mineralization within the Kizhnica–Hajvalia–Badovc ore field, including Cu–Bi±Ag±As sulfosalts paragenesis previously not described in Kosovo and in this part of the Vardar Zone. Chemical composition of Bi–Pb±Cu±Ag and Cu–Bi±Ag±As sulfosalts, sulfides, and associated minerals, as well as their paragenetic relationships and the distribution of minor and trace elements in main ore minerals, are discussed based on microscopy, microprobe, and laser ablation inductively coupled plasma mass spectrometry studies. The Cu–Bi–Ag±W hydrothermal mineralization in Janjevo was formed during four stages: (1) Early base metal stage, (2) Bismuth stage, (3) Main stage, and (4) Late stage. The Early base metal stage is represented by pyrite, sphalerite I, chalcopyrite I, galena I, bournonite I, tetrahedrite I, siderite, and quartz. The Bismuth stage includes arsenopyrite I, löllingite, native bismuth, galena II, chalcopyrite II, tetrahedrite II, quartz, siderite, and Bi–Pb±Cu±Ag sulfosalts: bismuthinite, aikinite, krupkaite, cosalite, and gustavite. The Main stage is represented by chalcopyrite III, tetrahedrite group minerals (tetrahedrite and tennantite) III, galena III, sphalerite II, arsenopyrite II, bournonite II, and siderite. The Cu–Bi±Ag±As sulfosalts (pearceite, cupropearceite, wittichenite, and an unknown phase: AgCuBiS₃) associated with galena IV, siderite, and quartz were formed in the final low-temperature Late stage. The application of GGIMF is geothermometry on sphalerite gives the following sphalerite precipitation temperatures: 220–272 °C for sphalerite I and 160–190 °C for sphalerite II. Presented results show that in addition to numerous Bi sulfosalts in Janjevo Cu–Bi–Ag±W ores, bismuth has been incorporated into base metal sulfides, as well as arsenopyrite. The main carrier of bismuth is arsenopyrite I, which has started the crystallization of the bismuth stage.

Keywords: bismuth, sulfosalts, tetrahedrite group minerals, AgCuBiS₃, LA-ICP-MS

Received: 4 October 2022; **accepted:** 13 February 2023; **handling editor:** J. Sejkora

The online version of this article (doi: 10.3190/jgeosci.371) contains supplementary electronic material.

1. Introduction

The Janjevo Cu–Bi–Ag±W mineralization is located in central Kosovo, about 10 km SE of the capital Prishtina (Fig. 1). It is situated in the southern part of the Trepça Mineral Belt (TMB), which is part of a major metallogenic zone, the Serbo-Macedonian metallogenic province (SMMP), part of the Western Tethyan metallogenic belt (Janković 1997; Borojević Šošarić et al. 2012; Baker 2019). The SMMP was formed during the late Oligocene to early Miocene post-collision extension and the associated intermediate to felsic magmatic activity with magmas of high-K, calc-alkaline to shoshonitic composition (Borojević Šošarić et al. 2012; Siron et al. 2016). The SMMP is predominantly known for the occurrence

of many Pb–Zn–Ag deposits (Strmić Palinkaš et al. 2013; Radosavljević et al. 2013; Kołodziejczyk et al. 2016a; Siron et al. 2016; Stojanović et al. 2018).

Polymetallic Pb–Zn–Ag deposits occur, for example, in the Kizhnica–Hajvalia–Badovc (KHB) ore field, which also includes the Janjevo Cu–Bi–Ag±W occurrence located in the eastern part of the ore field (Fig. 2). There are three major Pb–Zn–Ag deposits documented in this ore field. These deposits were mined in the 20th century. However, mining in the KHB ore field dates to Roman times, and many small-scale mining works are observed in the entire area. Short adits, dumps, and remnants of mining infrastructure in the eastern part of the KHB ore field suggest mining activity focused on different metals (mainly copper). Mineral occurrences in the eastern part

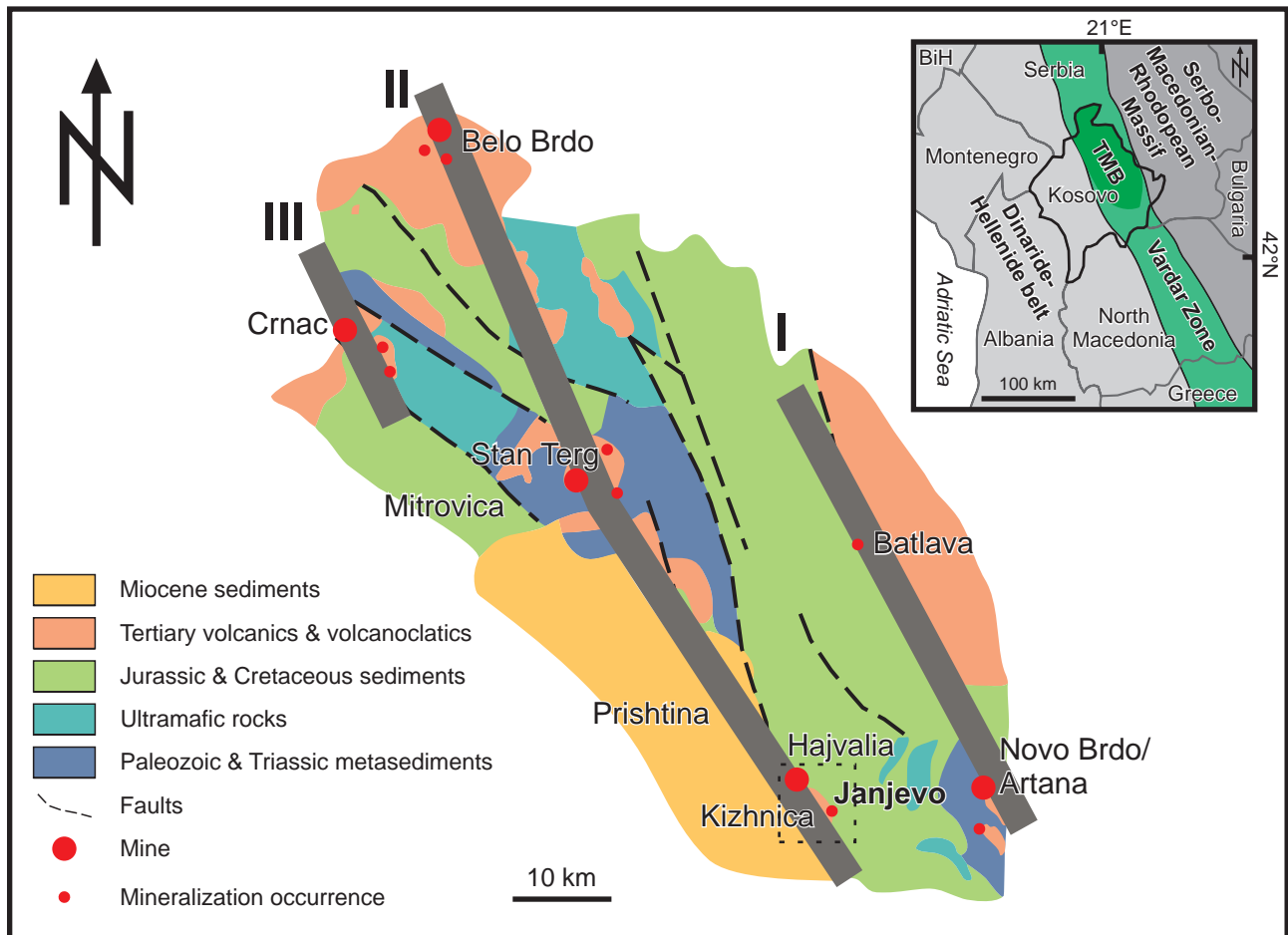


Fig. 1 – Simplified geological map of Vardar Zone and Trepča Mineral Belt (TMB) (modified after Hyseni et al. 2010; Strmić Palinkaš et al. 2013), the dashed-line square shows the Kizhnica–Hajvalia–Badovc ore field presented in Fig. 2. I = Batlava–Artana Zone, II = Belo Brdo–Stan Terg–Hajvalia Zone, III = Crnac Zone.

of the KHB ore field are associated with the Bi–Cu±Au metallogenic zone and their proximity to intrusive rocks have been described by Mederski et al. (2021a) (Fig. 2).

This work presents detailed mineralogical and geochemical characteristics of a newly discovered hydrothermal Cu–Bi–Ag±W mineralization in Janjevo, Kosovo. The chemical composition of Bi–Pb±Cu±Ag and Cu–Bi±Ag±As sulfosalts, sulfides, and associated minerals, as well as their paragenetic relationships and the distribution of minor and trace elements in main ore minerals, are presented. Special attention is given to the mineralogy of Bi-sulfosalts and the evolution and distribution of bismuth in the main ore minerals in the Cu–Bi–Ag±W ores from Janjevo.

2. Geological setting

The Janjevo area is part of the NW–SE trending Vardar Zone, which is bounded by the Dinarides, the Drina–Ivanjica Terrain, and the Pelagonian Zone to the west,

and the Serbo–Macedonian Massif to the east. The Vardar Zone is composed of Paleozoic–Triassic metamorphic rocks, Jurassic ophiolite complex (serpentinite and gabbro with minor sedimentary rocks), Jurassic and Cretaceous sedimentary complex (series of flysch, carbonate rocks, volcanic and volcanoclastic rocks), and Tertiary andesites, trachytes, latites, and felsic pyroclastic rocks (Janković 1995; Cvetković et al. 2004; Elezaj 2009; Borojević Šoštarić et al. 2012; Strmić Palinkaš et al. 2013) (Fig. 1). The Oligocene–Miocene polymetallic mineralization extends along the so-called Trepča Mineral Belt (TMB), which is related to the post-collisional calc-alkaline to shoshonitic magmatic activity accompanied by widespread hydrothermal activity (Janković 1995; Hyseni et al. 2010). Mineralization within the TMB is controlled by three NNW-trending regional fault zones: (I) Batlava–Artana Zone, (II) Belo Brdo–Stan Terg–Hajvalia Zone, and (III) Crnac Zone (Hyseni et al. 2010) (Fig. 1). The TMB region is dominated by hydrothermal Pb–Zn–Ag deposits: skarns, carbonate replacements, veins, breccias, veinlets, and disseminations in altered rocks such as

listvenites (Hyseni et al. 2010; Borojević Šošarić et al. 2011, 2013; Strmić Palinkaš et al. 2013; Radosavljević et al. 2015; Kołodziejczyk et al. 2015, 2016a, b, 2017; Mederski et al. 2019, 2021a, b, 2022b).

The oldest rocks in the KHB ore field belong to the Paleozoic–Triassic metasedimentary complex, composed of schists and marbles, which occur in the western part of the ore field (Fig. 2). In the central part of the area, an ultramafic complex of Triassic–Jurassic age is exposed, which is represented by gabbro, serpentized basalts, peridotites, and in places is altered by later hydrothermal fluids that formed carbonate listvenites (Mederski et al. 2019, 2021b). In the southern part of the area, there is a Jurassic *mélange* series with olistoliths, composed of various metamorphosed rocks in the greenschist facies, primarily sedimentary and mafic rocks. The eastern part of the area contains terrigenous rocks of Jurassic–Cretaceous age. The flysch series is represented by fining-upward sequences of conglomerates, silty-calcareous units, greywacke, sandy and silty lithologies, and calcareous sandstone to pebble conglomerates (Buerger and Giroux 2016). The youngest and most extensive units are Oligocene–Miocene volcanic and volcanoclastic rocks. Intrusive dikes and sills are represented by a hornblende-biotite porphyry andesite and a feldspar porphyry andesite (Buerger and Giroux 2016).

The Kizhnica–Hajvalia–Badovc (KHB) ore field shows a metallogenic zonation described by Mederski et al. (2021a) that may be related to a concealed porphyry system (Fig. 2). The central and western parts are characterized by the presence of a **Pb–Zn–Sb ± Ni zone**, and there are major documented Pb–Zn–Ag deposits in the KHB ore field, including Hajvalia, Badovc, and Kizhnica (Fig. 2). The Hajvalia carbonate replacement Pb–Zn–Ag deposit is hosted in Paleozoic formations (marbles

and schists), while the Kizhnica Pb–Zn–Ag deposit is located on the contact between serpentinites and flysch series, and forms veins, lenses, and disseminations (Dangić 1985; Kołodziejczyk et al. 2016a). The Badovc Pb–Zn–Ag deposit occurs in the form of banded-veins, veinlets, and disseminations within the listvenites (Mederski et al. 2019, 2021b, 2022b). In the southern part of the area, there is a distal **Sb–As–Tl–Hg zone** (Fig. 2), where a low-temperature sediment-hosted As–Sb–Tl–Pb ± Hg ± Au mineralization occurs within Triassic marbles in Janjevo (Mederski et al. 2022a, 2022b). Mineralization associated with the **Bi–Cu ± Au zone** is known from a few minor occurrences in the eastern part of the KHB ore field. Epithermal Cu–Bi veinlets and veinlets with Bi sulfosalts are observed within the Kizhnica andesite (Mederski et al. 2021a). In the NE part of the area, Bi–Au–Cu–Te mineralization with Bi sulfosalts hosted

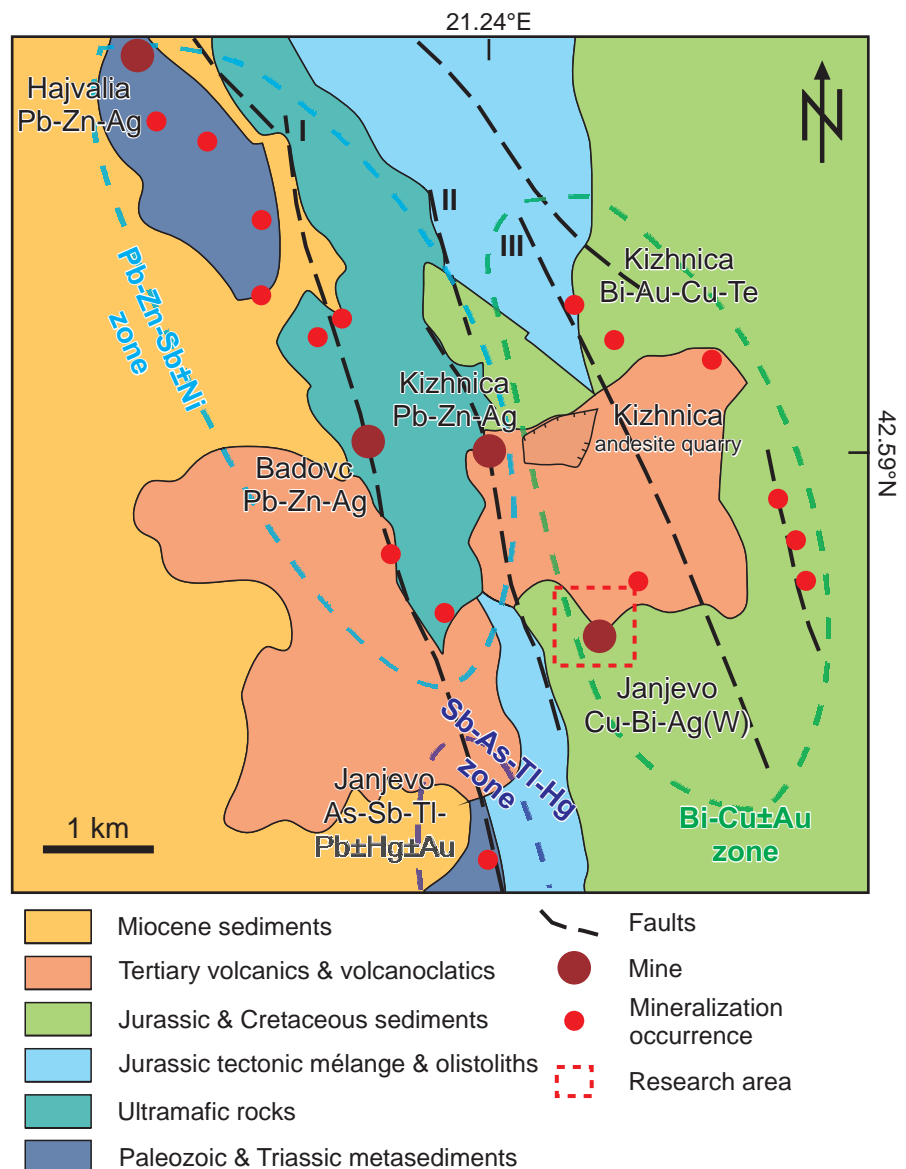


Fig. 2 – Simplified geological map of the Kizhnica–Hajvalia–Badovc ore field. Abbreviations: I = Hajvalia–Badovc Tectonic Zone; II = Kizhnica Tectonic Zone; III = Okosnica Tectonic Zone.

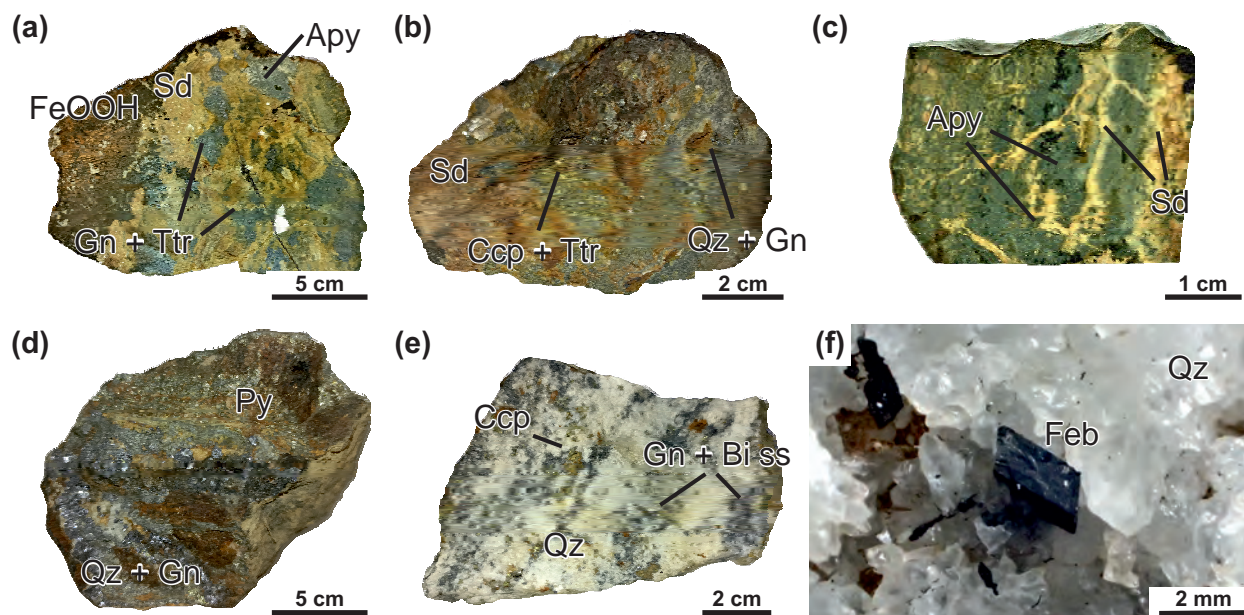


Fig. 3 – Representative photographs of the Cu–Bi–Ag±W ores from Janjevo. **a–d** – Polymetallic siderite ore with arsenopyrite, tetrahedrite, galena, chalcocopyrite, and quartz. **e** – Quartz ore with galena, chalcocopyrite, and Bi sulfosalts. **f** – Euhedral wolframite (ferberite) crystal from quartz druse. Apy – arsenopyrite, Bi ss – bismuth sulfosalts, Ccp – chalcocopyrite, Feb – ferberite, FeOOH – Fe hydroxides, Gn – galena, Py – pyrite, Sd – siderite, Qz – quartz, Ttr – tetrahedrite.

by hornfels between flysch and andesite intrusions was previously described by Mederski et al. (2021a). Similar mineralization is documented in the Slivovo Au–Ag deposit east of the KHB ore field (Buerger and Giroux 2016). In the SE part of the KHB ore field, the Janjevo Cu–Bi–Ag±W mineralization occurs at the contact between the flysch series and andesites (Westner 2017; Mederski et al. 2021c).

3. Locality and investigated material

Material for the study was collected from small historical waste piles on one of the hills between the Janjevo village and the Kizhnica andesite quarry. Mineralized ore samples with Cu–Bi–Ag±W association were found close to the entrance of a backfilled adit. The GPS coordinates of the sampling site are 42°34'57.92"N, 21°15'1.54"E. Outcrops with altered andesites have been observed in the close vicinity. In addition, flysch series rocks were noticed at the entrance of the drainage adit, which is inaccessible due to the clenching of siltstone rocks. The ore from Janjevo is coarse-grained, composed primarily of siderite (Fig. 3a–b), which is replaced by iron hydroxides due to weathering. Within the siderite ores are numerous polymetallic aggregates of up to several cm in size, composed of arsenopyrite, pyrite, chalcocopyrite, galena, and tetrahedrite (Fig. 3a–d). In addition, there are banded siderite-arsenopyrite ores (Fig. 3c), as well as quartz ores

with aggregates of galena, chalcocopyrite, and Bi sulfosalts (Fig. 3e). Tiny wolframite crystals up to a few mm in size were observed in the quartz druses (Fig. 3f).

4. Methods

Samples from the Janjevo Cu–Bi–Ag±W locality were examined macroscopically, and based on visual evaluation, a number of 27 thin and polished sections were prepared for mineralogical research. Mineral assemblages and textural relationships were studied using reflected and transmitted light microscopy. The quantitative element composition of sulfides, sulfosalts, and other associated minerals was obtained in 10 samples representing major types of mineralization using electron probe microanalysis (EPMA). Trace element composition of selected minerals (pyrite, sphalerite, chalcocopyrite, arsenopyrite, and tetrahedrite group minerals) was determined by laser ablation inductively coupled plasma mass spectrometry (LA-ICP-MS) in four samples.

Quantitative chemical analyses of sulfides, sulfosalts, and other associated minerals were performed on a JEOL Super Probe 8230 electron microprobe (Kraków, Poland: Laboratory of Critical Elements at Faculty of Geology, Geophysics, and Environmental Protection, AGH-UST), operating in the wavelength-dispersive (WDS) mode (20 kV [exception wolframite: 15 kV], 20 nA [exception pearceite–cupropearceite: 10 nA], and 1–2 μm wide

beam). The following standards, X-ray lines, and detection limits (in wt. %) for the minerals measured (pyrite, arsenopyrite, löllingite, tetrahedrite group minerals, Bi and Ag sulfosalts, galena, wolframite, and siderite) are summarized in Tab. S1 (ESM 1). Microprobe microanalyses were conducted for the determination of iron, copper, and zinc contents used as internal standards during LA-ICP-MS analyses for pyrite (Fe), chalcopyrite (Fe), arsenopyrite (Fe), tetrahedrite group minerals (Cu), and sphalerite (Zn).

Trace element concentrations in pyrite, sphalerite, chalcopyrite, arsenopyrite, and tetrahedrite group minerals were measured using a PerkinElmer ELAN DRC-e ICP mass spectrometer combined with a New Wave UP193-FX excimer laser ablation system at the Geological Institute, Bulgarian Academy of Sciences, Sofia, Bulgaria. The ablation was conducted in He medium. To maximize sensitivity, the ICP-MS was optimized daily concerning the oxide production rate of ThO/Th (0.5 %). Operating conditions of the laser system include a 6 Hz repetition rate; 20 to 35 µm spot size; and energy density on analyzed minerals and standards of 3.3–3.4 J/cm² (at 35 µm spot), 3.1 J/cm² (at 25 µm spot), and 2.9–3.0 J/cm² (at 20 µm spot). The nebulizer gas flow rate was 0.8 L/min, while auxiliary and make-up gas flow rates were 0.92 L/min. The analysis time was 100 s (background: 40 s, laser-on the sample: 60 s). The acquisition dwells time was set to 0.02 s for ⁷¹Ga, ⁷⁴Ge, ¹⁰⁷Ag, ¹²⁵Te, ²⁰²Hg, ²⁰⁵Tl; to 0.03 s for ¹¹⁵In, ¹¹⁸Sn; to 0.04 s for ¹⁹⁷Au, and 0.01 s for all other monitored isotope masses – ³⁴S, ⁴⁹Ti, ⁵¹V, ⁵³Cr, ⁵⁵Mn, ⁵⁷Fe, ⁵⁹Co, ⁶⁰Ni, ⁶⁵Cu, ⁶⁶Zn, ⁷¹Ga, ⁷⁴Ge, ⁷⁵As, ⁸²Se, ⁹⁵Mo, ¹⁰⁷Ag, ¹¹¹Cd, ¹¹⁵In, ¹¹⁸Sn, ¹²¹Sb, ¹²⁵Te, ¹⁸¹Ta, ¹⁸²W, ¹⁹⁷Au, ²⁰²Hg, ²⁰³Tl, ²⁰⁸Pb, and ²⁰⁹Bi. Targeted areas in the polished sections were predefined to avoid obvious mineral inclusions. Repeated external standardization was conducted by analyzing NIST SRM 610 glass standard and the USGS Mass 1 sulfide standard. Data reduction was made using SILLS software (Guillong et al. 2008). During data reduction, peak-shaped fluctuations of the intensity signal of some isotopes were investigated to exclude the influence of other minerals on the chemical composition of the studied minerals. Limits of detection for each isotope mass are determined for every analysis and may differ.

5. Results

5.1. Paragenetic sequence

The Cu–Bi–Ag±W hydrothermal mineralization in Janjevo was formed during four main stages (Fig. 4): (1) Early base metal stage, (2) Bismuth stage, (3) Main stage, and (4) Late stage. Each stage contains different generations

of sphalerite, chalcopyrite, galena, bournonite, and tetrahedrite group minerals, that have been distinguished based on textural features and the geochemistry of trace elements. The first stage is represented by sulfides: pyrite, sphalerite I, chalcopyrite I, galena I, and sulfosalts: bournonite I, and tetrahedrite I. The main gangue minerals are siderite and quartz. The second Bi-dominated stage begins with the crystallization of arsenopyrite and traces of löllingite and native bismuth. Numerous Bi–Pb±Cu±Ag sulfosalts represented by bismuthinite, aikinite, krupkaite, cosalite, and gustavite were crystallized subsequently with quartz, galena II, chalcopyrite II, and tetrahedrite II. The main productive stage of precipitation includes chalcopyrite III, tetrahedrite group minerals (tetrahedrite and tennantite) III, galena III, sphalerite II, arsenopyrite II, bournonite II, and siderite. Texture observations suggest that the Cu–Bi±Ag±As sulfosalts (pearceite, cupropearceite, wittichenite, and an unknown phase: AgCuBiS₃) associated with galena IV, siderite, and quartz, were formed in the final low-temperature Late stage in Janjevo.

5.2. Mineralogy and textures

EPM analyses of sulfides, sulfarsenides, diarsenides, and associated minerals are presented in Tab. S2 (ESM 2), while sulfosalts analyses are presented in Tab. S3 (ESM 3).

5.2.1. Sulfides

Pyrite is a minor sulfide in ores from Janjevo and crystallized during the first early base metal stage (Fig. 4). It forms euhedral crystals up to 200 µm in size or larger subhedral aggregates up to 600 µm (Fig. 5a). Pyrite crystals often host numerous inclusions of younger galena, arsenopyrite, or sphalerite. In addition, younger sulfides very often overgrow pyrite crystals (Fig. 5a). The formula of pyrite from Janjevo can be expressed as (Fe_{0.97–1.00} Ni_{0.00–0.03})_{Σ1.00}(S_{1.94–2.05}As_{0.00–0.05})_{1.98–2.05}.

Sphalerite is a common sulfide at Janjevo and occurs in two generations. Sphalerite I forms irregular aggregates up to 2 mm in size that crystallized during the first early base metal stage (Fig. 5b, c). This sphalerite contains numerous chalcopyrite exsolutions (chalcopyrite I) (Fig. 5b) at the rims and is overgrown by younger galena I. It is characterized by high iron concentration (Fe up to 0.19 *apfu*), with iron-dependent oscillatory zonation visible in BSE images (Fig. 5c). A generalized formula for sphalerite I is (Zn_{0.80–0.98}Fe_{0.02–0.19})_{Σ1.00}S_{0.99–1.05}. Sphalerite II crystallized during the third, main stage (Fig. 4), forming aggregates of up to 500 mm in size. It occurs mainly in association with chalcopyrite III (Fig. 5d), and is characterized by significantly lower iron concentration (up to 0.03 *apfu*), compared with sphalerite I. The

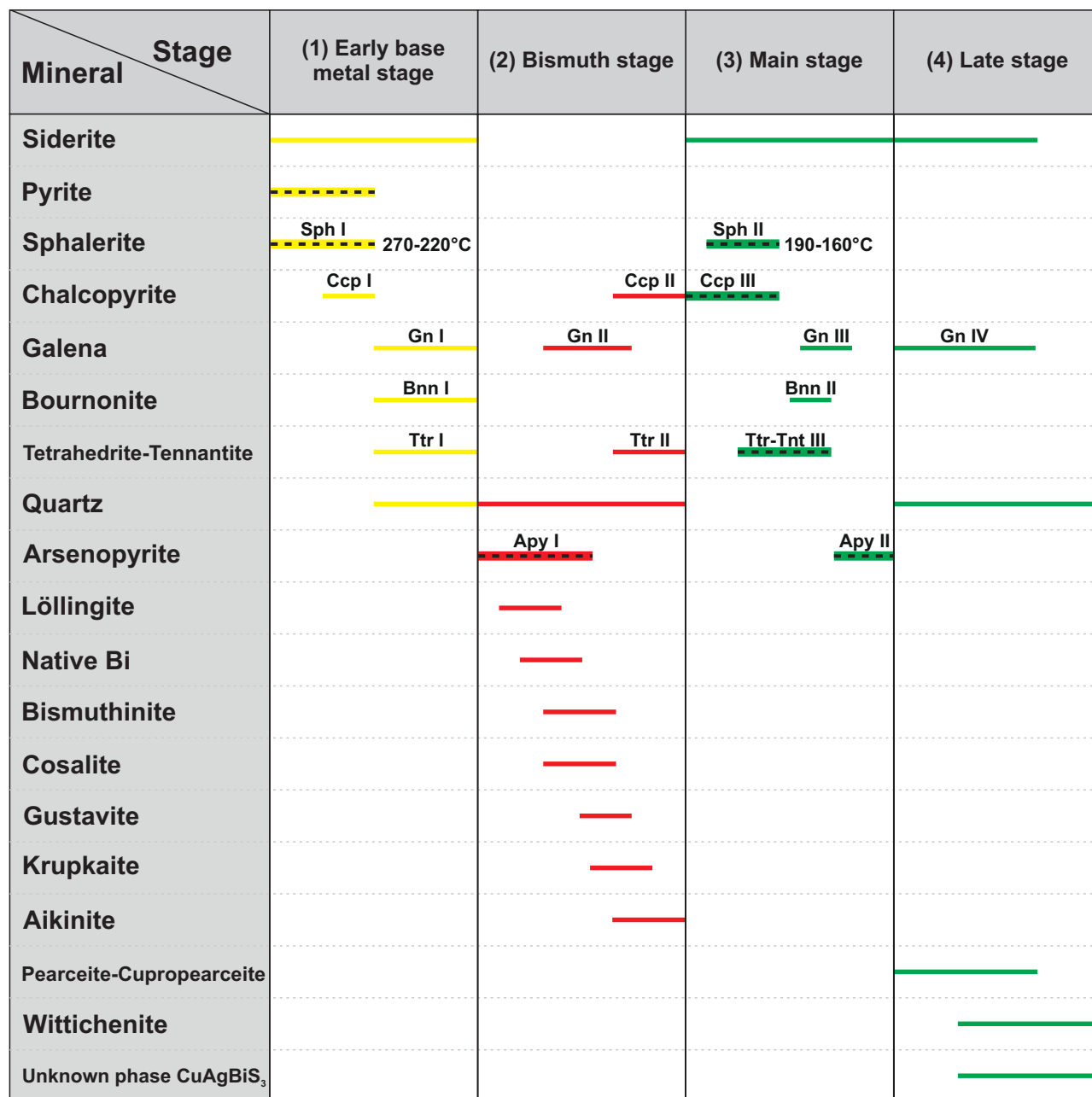


Fig. 4 – Formation stages and paragenetic sequence of Cu–Bi–Ag±W mineralization from the Janjevo. The dashed lines indicate specific generations of minerals that were measured by the LA-ICP-MS technique.

formula of sphalerite II can be expressed as $(Zn_{0.95-0.99}Fe_{0.01-0.03}Ga_{0.00-0.01})_{\Sigma 1.00}S_{0.97-1.02}$.

Chalcopyrite is the most common sulfide in the studied samples, and occurs in three stages, chalcopyrite I, II and III. Chalcopyrite I occurs as exsolutions and minor inclusions in sphalerite I (Fig. 5b). In contrast, chalcopyrite II co-crystallized with aikinite (Fig. 6h). The most abundant generation is chalcopyrite III that formed in the main precipitation stage (Fig. 4). It is found in aggregates with tetrahedrite, galena, and sphalerite up to several cm in size (Fig. 5d–f). Occasionally it forms euhedral crystals

at the rims of the aggregates. The chemical compositions of all generations of chalcopyrite correspond almost to the ideal stoichiometry of this mineral phase with the formula: $(Cu_{0.98-0.99}Fe_{0.01-0.02})_{\Sigma 2.00}S_{1.97-2.06}$.

Galena is widespread in the ore and is found in all four stages of precipitation, and occurs in four generations, galena I, II, III, and IV (Fig. 4). Galena I overgrows sphalerite I, but also forms larger aggregates up to 2 μm (Fig. 5b–c). In addition, tetrahedrite and bournonite inclusions are observed within galena I. Galena II is associated with Bi sulfosalts: bismuthinite and cosalite

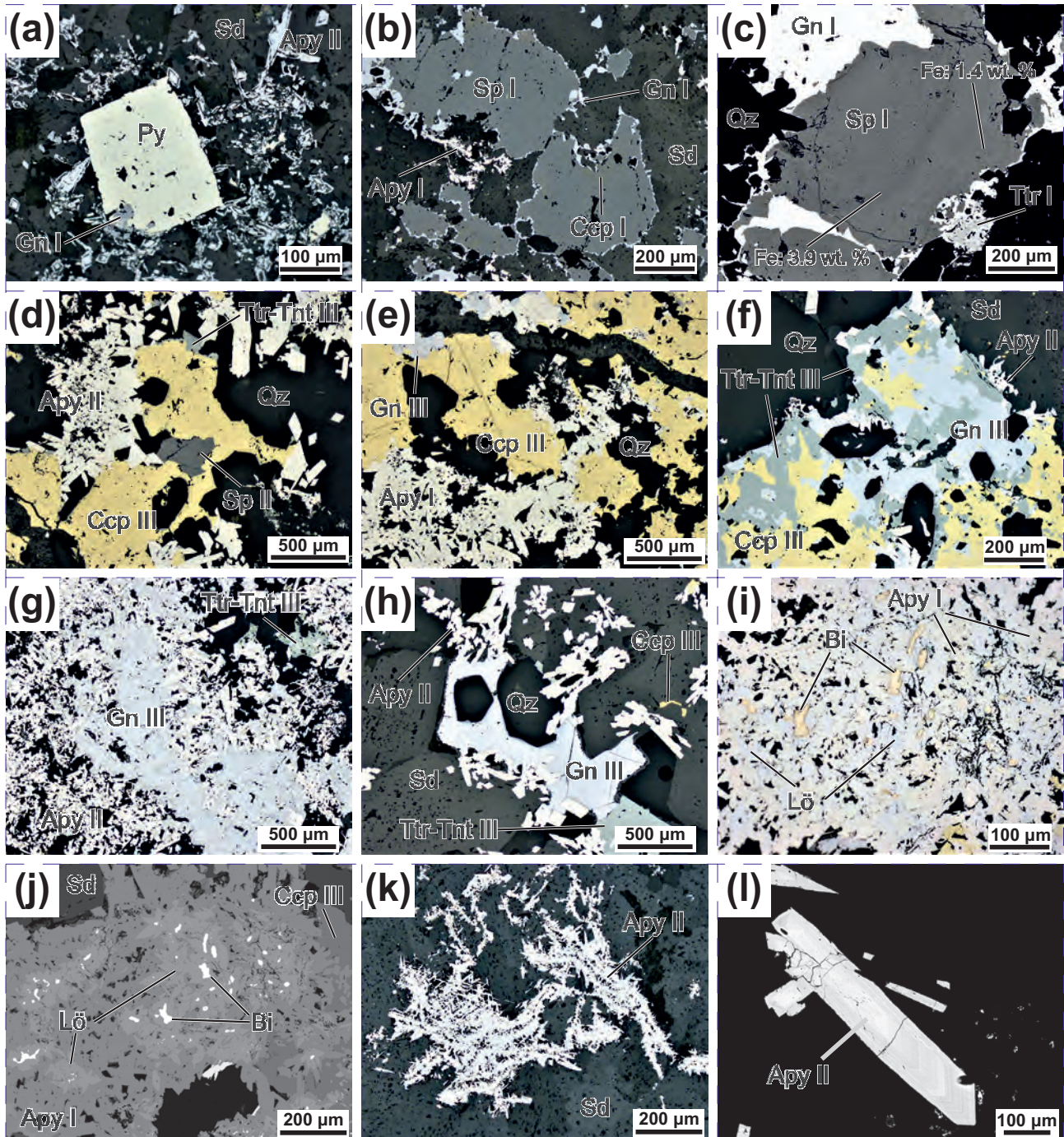


Fig. 5 – Reflected-light photomicrographs (a–b, d–i, k) and back-scattered electron (BSE) images (c, j, l) of Cu–Bi–Ag±W mineralization from the Janjevo. **a** – Euhedral pyrite crystal is overgrown by younger galena and arsenopyrite II, siderite. **b** – Aggregates of sphalerite I with exsolutions of chalcopyrite I have overgrown by arsenopyrite and galena, siderite. **c** – Oscillatory zonation in sphalerite I related to variable Fe content, overgrown by galena I and tetrahedrite I, quartz. **d** – Typical coarse-crystalline aggregates composed of chalcopyrite III, sphalerite II and tetrahedrite-tennantite III overgrown by arsenopyrite II, quartz. **e** – Arsenopyrite I associated with aggregates composed of chalcopyrite III and galena III, quartz. **f** – Typical polymineralic aggregates chalcopyrite III–tetrahedrite–tennantite III–galena III overgrown by arsenopyrite II, siderite, and quartz. **g** – Coarse-crystalline galena III with tetrahedrite-tennantite III and arsenopyrite II. **h** – Galena III with tetrahedrite-tennantite III and arsenopyrite II filling the cavity between euhedral crystals of siderite and quartz, chalcopyrite III. **i** – Disintegration textures of arsenopyrite I–löllingite aggregates with visible droplets of native bismuth. **j** – Disintegration textures of arsenopyrite I–löllingite aggregates with visible droplets of native bismuth in euhedral löllingite crystals, chalcopyrite III. **k** – Skeletal aggregates of arsenopyrite II in siderite. **l** – An elongated euhedral crystal of arsenopyrite II. Apy – arsenopyrite, Bi – native bismuth, Ccp – chalcopyrite, Gn – galena, Lö – löllingite, Py – pyrite, Qz – quartz, Sd – siderite, Sp – sphalerite, Tnt – tennantite, Ttr – tetrahedrite.

(Fig. 5f), and forms aggregates of up to 2 mm. Galena II shows elevated contents of Bi (up to 0.03 *apfu*). Galena III very commonly overgrows chalcopyrite–tetrahedrite aggregates (Fig. 5f), as well as arsenopyrite I (Fig. 5g–h). It forms crystals up to 3 mm, which are characterized by only minor concentrations in Bi (up to 0.01 *apfu*), the formula of galena III can be expressed as $(\text{Pb}_{0.97-1.00}\text{Sb}_{0.00-0.02}\text{Bi}_{0.00-0.01})_{\Sigma 1.00}\text{S}_{0.96-0.98}$. The youngest galena IV co-crystallized with Ag minerals: pearceite and wittichenite, and is characterized by high concentrations of Bi (up to 0.10 *apfu*) and Ag (up to 0.06 *apfu*), the formula of galena IV can be expressed as $(\text{Pb}_{0.78-0.87}\text{Bi}_{0.06-0.10}\text{Ag}_{0.03-0.06}\text{Cu}_{0.03-0.05}\text{Fe}_{0.01-0.02})_{\Sigma 1.00}\text{S}_{0.95-0.96}$.

5.2.2. Sulfarsenides + diarsenides

Arsenopyrite is the most common ore mineral in the studied samples, and two generations are observed, arsenopyrite I and II (Fig. 4). Arsenopyrite I forms aggregates up to several mm in size, composed of euhedral arsenopyrite crystals, very often accompanied by löllingite (Fig. 5i–j). These aggregates are commonly corroded and are overgrown by the ore minerals of the younger mineralization, abundant in tetrahedrite, chalcopyrite, and galena. In addition, large aggregates of arsenopyrite I with löllingite often show the presence of irregular native Bi blebs inside (Fig. 5i–j). The formula of arsenopyrite I can be expressed as $\text{Fe}_{1.00}(\text{As}_{0.85-1.01}\text{Sb}_{0.00-0.03}\text{Bi}_{0.00-0.01})_{\Sigma 0.88-1.01}\text{S}_{0.95-1.06}$. Arsenopyrite from Janjevo shows elevated Sb concentration up to 0.03 *apfu* in arsenopyrite I and II. Arsenopyrite II postdates all the other sulfides at the main stage, apart from galena IV (Fig. 4). It mainly forms characteristic euhedral crystals (Fig. 5k–l), sometimes growing on older sulfides (Fig. 5f, h). The formula of arsenopyrite II can be expressed as $\text{Fe}_{1.00}(\text{As}_{0.87-0.96}\text{Sb}_{0.00-0.03})_{\Sigma 0.90-0.97}\text{S}_{0.95-1.05}$.

Löllingite co-crystallized with arsenopyrite I and forms euhedral to subhedral crystals up to 100 μm (Fig. 5i–j). There are no isolated crystals of löllingite, but it always forms aggregates with arsenopyrite I. In addition, irregular native Bi droplets are observed within the aggregates (Fig. 5i–j). A generalized formula for löllingite is $\text{Fe}_{1.00}(\text{As}_{1.85-1.93}\text{S}_{0.01-0.09})_{\Sigma 1.93-1.99}$.

5.2.3. Sulfosalts

The **tetrahedrite group minerals** are widespread and are the most common sulfosalts in the Janjevo ores. Minerals of this group crystallized during the first three hydrothermal stages (Fig. 4). Tetrahedrite I co-crystallized with galena I and bournonite I, and forms irregular aggregates up to 150 μm (Fig. 5c; 6a). According to the recently published nomenclature scheme of minerals of the tetrahedrite group (Biagioni et al. 2020), tetrahedrite I is represented by Sb members with mixed Fe and Zn

concentrations at the C structural position: tetrahedrite-(Fe) predominates, only one analysis can be classified as tetrahedrite-(Zn) (Fig. 7a–b). In addition, tetrahedrite I has the highest Ag values of all generations: 0.46–0.97 *apfu* (Fig. 7c). A generalized formula for tetrahedrite-(Fe) (tetrahedrite I generation) based on 16 cations is $(\text{Cu}_{9.02-9.53}\text{Ag}_{0.46-0.95}\text{Fe}_{1.06-1.47}\text{Zn}_{0.50-1.04})_{\Sigma=11.95-12.15}(\text{Sb}_{2.09-3.91}\text{As}_{0.08-1.79}\text{Bi}_{0.00-0.06})_{\Sigma=3.85-4.05}\text{S}_{12.74-13.09}$. Tetrahedrite II occurs in association with chalcopyrite, aikinite, galena II, and gustavite. All analyses fall on tetrahedrite-(Fe) (Fig. 7d), and a generalized formula for tetrahedrite II based on 16 cations is $(\text{Cu}_{9.32-9.61}\text{Ag}_{0.37-0.56}\text{Fe}_{1.46-1.60}\text{Zn}_{0.40-0.63})_{\Sigma=11.93-12.01}(\text{Sb}_{3.29-3.83}\text{As}_{0.12-0.64}\text{Bi}_{0.04-0.13})_{\Sigma=3.99-4.07}\text{S}_{13.08-13.39}$. Tetrahedrite II also shows minor enrichment in Ag (up to 0.56 *apfu*) (Fig. 7c). Tetrahedrite–tennantite III is abundant in the ore from Janjevo. It forms sizable irregular aggregates associated with chalcopyrite III, sphalerite II, and galena III, and the aggregates, or euhedral crystals, sometimes reach up to 1 cm (Fig. 5f–g; 6b). This generation is characterized by significant chemical variability at positions C (Fe–Zn) (Fig. 7b) as well as D (Sb–As) (Fig. 7a). In this generation, the four members of the tetrahedrite group minerals are represented by tetrahedrite-(Fe), tetrahedrite-(Zn), tennantite-(Fe), and tennantite-(Zn) (Fig. 7d). The considerable chemical variability (especially related to Sb–As substitution) contributes to the significant zonal variability seen in BSE images: oscillatory (Fig. 6c–e) as well as irregular (Fig. 6e). The presence of the end members of the tetrahedrite group also influences their differentiation by optical features visible under the microscope in reflected light: stoichiometric tetrahedrite is olive green, while stoichiometric tennantite shows a bluish tint (Fig. 6b). In addition, tetrahedrite–tennantite III shows slight enrichments at the C position: Hg (up to 0.24 *apfu*), Pb (up to 0.02 *apfu*), and Mn (up to 0.01 *apfu*), and at the D position: Bi (up to 0.31 *apfu*). A generalized formula for tetrahedrite–tennantite III based on 16 cations is: $(\text{Cu}_{9.49-10.04}\text{Ag}_{0.04-0.47}\text{Fe}_{1.00-1.86}\text{Zn}_{0.09-1.05}\text{Hg}_{0.00-0.01}\text{Pb}_{0.00-0.01}\text{Mn}_{0.00-0.01})_{\Sigma=11.92-12.42}(\text{Sb}_{1.80-3.95}\text{As}_{0.02-1.90}\text{Bi}_{0.00-0.31})_{\Sigma=3.58-4.08}\text{S}_{12.52-13.47}$ for tetrahedrite-(Fe), $(\text{Cu}_{9.49-10.18}\text{Ag}_{0.02-0.32}\text{Zn}_{0.99-1.84}\text{Fe}_{0.16-0.99}\text{Hg}_{0.00-0.06}\text{Pb}_{0.00-0.02})_{\Sigma=11.85-12.43}(\text{Sb}_{1.79-3.91}\text{As}_{0.12-1.94}\text{Bi}_{0.01-0.21})_{\Sigma=3.57-4.15}\text{S}_{12.71-13.44}$ for tetrahedrite-(Zn), $(\text{Cu}_{9.82-10.10}\text{Ag}_{0.01-0.29}\text{Fe}_{0.99-1.95}\text{Zn}_{0.05-0.96}\text{Hg}_{0.00-0.01}\text{Pb}_{0.00-0.01})_{\Sigma=11.83-12.46}(\text{As}_{1.75-4.15}\text{Sb}_{0.00-1.79}\text{Bi}_{0.00-0.26})_{\Sigma=3.54-4.17}\text{S}_{12.77-13.55}$ for tennantite-(Fe), and $(\text{Cu}_{9.83-10.15}\text{Ag}_{0.01-0.12}\text{Zn}_{0.99-1.21}\text{Fe}_{0.79-1.02}\text{Pb}_{0.00-0.01})_{\Sigma=11.86-12.17}(\text{As}_{2.32-3.98}\text{Sb}_{0.14-1.65}\text{Bi}_{0.01-0.09})_{\Sigma=3.83-4.14}\text{S}_{12.71-13.21}$ for tennantite-(Zn).

Sulfosalts of the **bismuthinite–aikinite series** are common in Janjevo paragenesis. Three members of this series: bismuthinite, krupkaite, and aikinite were identified (Fig. 8; 9). Precise identification was based on a calculation of the degree of aikinite substitution (n_{aik}): $(\text{Bi}^{3+} + \square \leftrightarrow \text{Pb}^{2+} + \text{Cu}^+)$ proposed by Topa et al. (2002). The value of n_{aik} was calculated following the scheme: $n_{\text{aik}} = 25(x+y)/2$, where x is the number of Cu atoms and

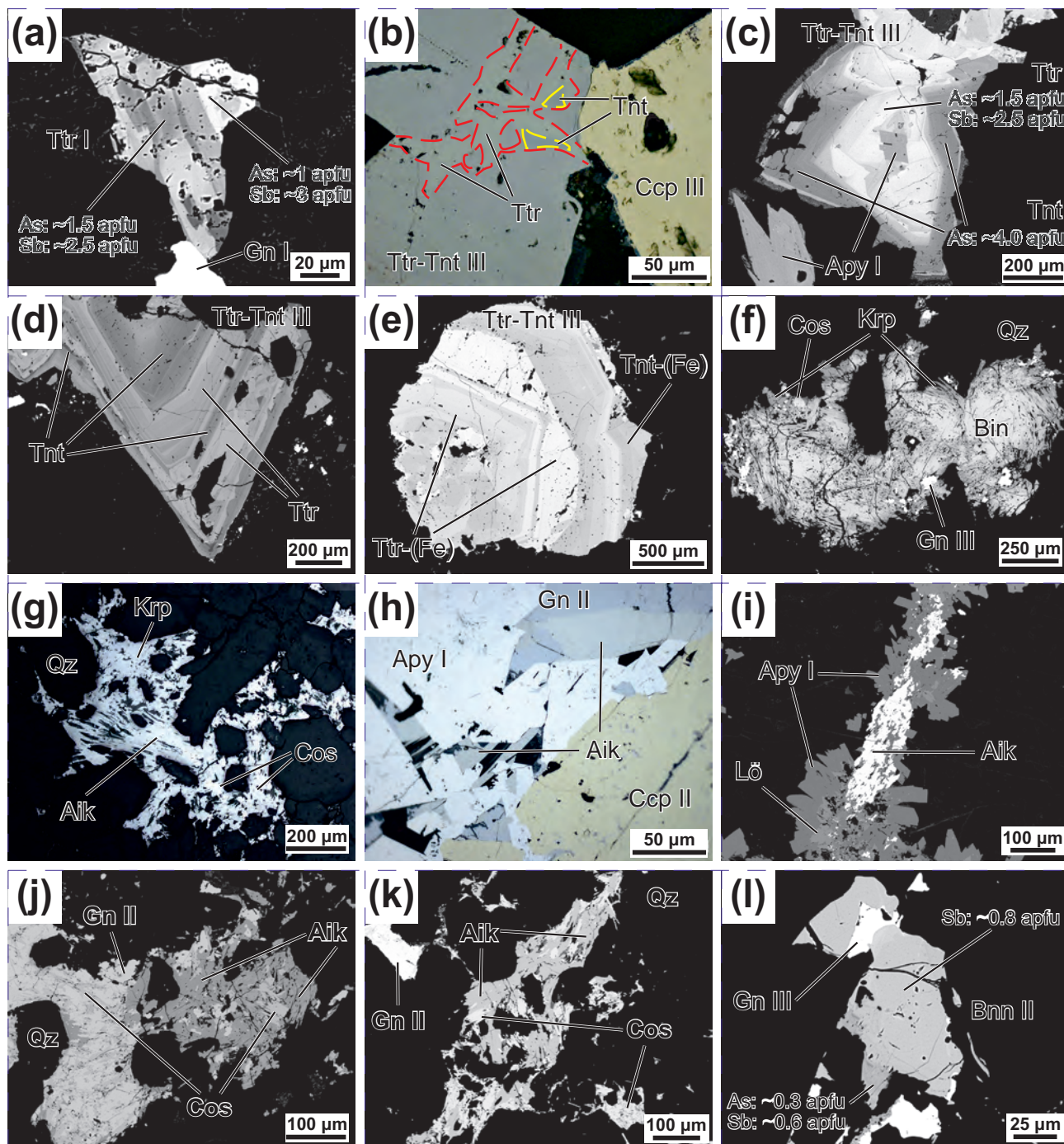


Fig. 6 – Reflected-light photomicrographs (**b, g–h**) and back-scattered electron (BSE) images (**a, c–f, i–l**) of sulfosalts from the Janjevo. **a** – Irregular zonation in tetrahedrite I. **b** – Tetrahedrite–tennantite III aggregate with chalcopyrite. The difference in optical characteristics between olive green stoichiometric tetrahedrite and stoichiometric tennantite with a blue tint is visible in reflected light. **c** – Oscillatory zonation in tetrahedrite–tennantite III aggregates, elongated arsenopyrite I crystals. **d** – Oscillatory and irregular zonation in a euhedral tetrahedrite–tennantite crystal III. **e** – Oscillatory and irregular zonation in a euhedral tetrahedrite–tennantite crystal III. **f** – In quartz ore, a polyminerale aggregate composed of bismuthinite, krupkaite, cosalite, and galena II. **g** – Elongated aikinite, cosalite, and krupkaite crystals fill the void between quartz crystals. **h** – Aikinite crystals are associated with chalcopyrite II, galena II, and arsenopyrite I. **i** – Elongated aikinite aggregates in association with arsenopyrite I and löllingite. **j** – Aikinite–cosalite aggregates in association with galena II and quartz. **k** – Elongated aikinite–cosalite crystals accompanied by galena II and quartz. **l** – A bournonite II crystal with an outer rim enriched in arsenic, accompanied by galena III. Aik – aikinite, Apy – arsenopyrite, Bin – bismuthinite, Bnn – bournonite, Ccp – chalcopyrite, Cos – cosalite, Gn – galena, Krp – krupkaite, Lö – löllingite, Qz – quartz, Tnt – tennantite, Ttr – tetrahedrite.

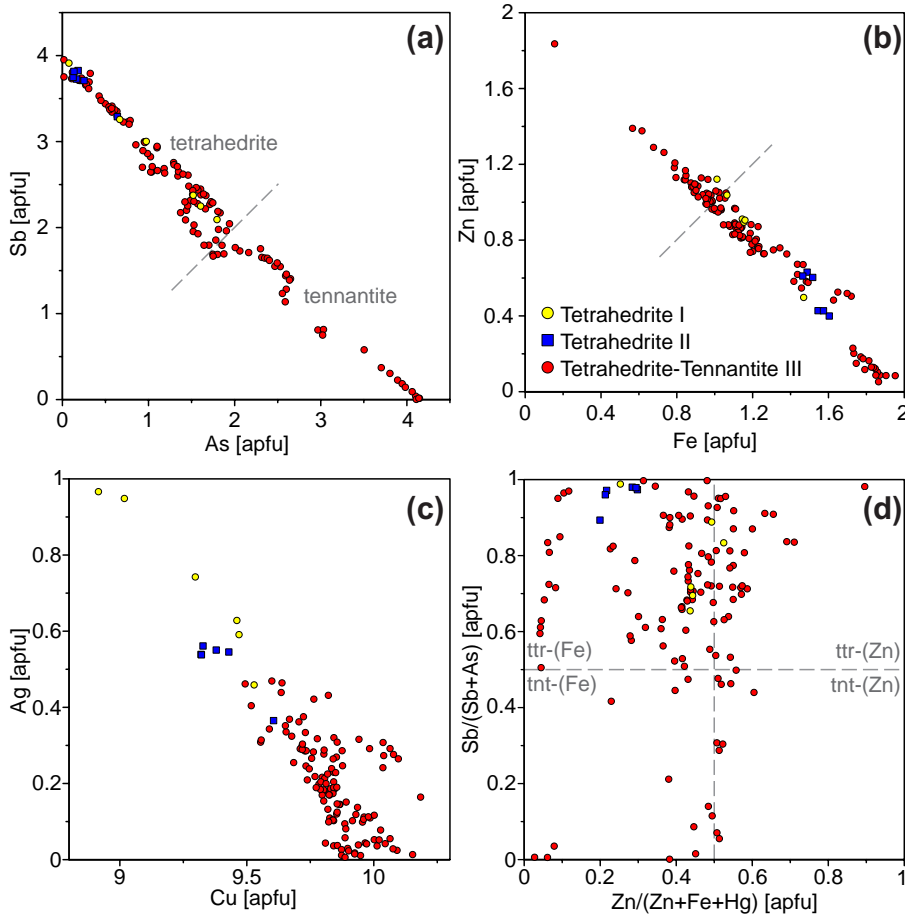


Fig. 7 – Compositional relationships in the tetrahedrite group minerals (TGM) from the Janjevo. **a** – Sb vs. As binary plot (*apfu*). **b** – Zn vs. Fe binary plot (*apfu*). **c** – Ag vs. Cu binary plot (*apfu*). **d** – Sb/(Sb+As) vs. Zn/(Zn+Fe+Hg) binary plot (*apfu*) after Biagioni et al. (2020).

y is the number of Pb atoms in the formulae, based on the sum $Ag + Bi + Sb + Fe + As + (Pb + Cu)/2 = 8$ atoms.

Bismuthinite is rare in the studied samples and is the oldest mineral of the bismuthinite-aikinite series in the Janjevo ores. It occurs only in quartz in association with other Bi sulfosalts (aikinite, krupkaite, cosalite), which overgrow bismuthinite crystals up to 400 μm in size (Fig. 6f). The degree of aikinite type substitution (n_{aik}) in bismuthinite from Janjevo is 0.24–6.80 (Tab. S3; Fig. 8). The empirical formula for studied bismuthinite can be expressed as $(\text{Bi}_{7.70-7.98}\text{Pb}_{0.00-0.31}\text{Cu}_{0.00-0.31}\text{Fe}_{0.00-0.01}\text{As}_{0.00-0.02}\text{Sb}_{0.01})_{\Sigma 8.01-8.27}\text{S}_{11.94-12.31}$.

Krupkaite is rare in the studied samples and was found in aggregates up to 30 μm in size. It forms intergrowths with bismuthinite and cosalite (Fig. 6f, g), with gustavite, or tiny inclusions in quartz. The degree of aikinite type substitution (n_{aik}) in krupkaite from Janjevo is 50.14–56.54 (Tab. S3; Fig. 8). The empirical formula for studied krupkaite can be expressed as $(\text{Cu}_{2.10-2.26}\text{Pb}_{1.92-2.16}\text{Fe}_{0.01-0.10}\text{Ag}_{0.00-0.02}\text{Bi}_{5.66-5.87}\text{Sb}_{0.01-0.11}\text{As}_{0.00-0.02})_{\Sigma 10.01-10.17}\text{S}_{11.54-12.19}$. It contains traces of Sb (up to 0.11 *apfu*).

Aikinite is the most common member of bismuthinite–aikinite series occurring in the ore from Janjevo. It forms elongated crystals up to 400 μm in size and is spatially

associated with other Bi sulfosalts (bismuthinite, cosalite, and krupkaite) and sulfides (chalcopyrite II and galena II) (Fig. 6g–k). The empirical formula for studied aikinite can be expressed as $(\text{Cu}_{3.00-3.93}\text{Pb}_{3.21-3.89}\text{Fe}_{0.00-0.28}\text{Ag}_{0.00-0.04}\text{Bi}_{4.02-4.78}\text{Sb}_{0.00-0.08}\text{As}_{0.00-0.05})_{\Sigma 11.16-11.88}\text{S}_{10.60-12.40}$, while the degree of aikinite type substitution is 82.33–99.29 (Tab. S3; Fig. 8). It contains traces of Sb (up to 0.08 *apfu*) and Fe (up to 0.28 *apfu*).

Cosalite occurs as intergrowths with bismuthinite, krupkaite, and aikinite or with galena in quartz (Fig. 6f–g, j–k). It forms needle-like crystals up to 300 μm long. The empirical formula for studied cosalite based on 20 anions (Topa and Makovicky 2010) can be expressed as $(\text{Cu}_{0.87-1.33}\text{Ag}_{0.19-0.38})_{\Sigma 1.06-1.63}(\text{Pb}_{6.93-7.45}\text{Fe}_{0.00-0.27})_{\Sigma 6.93-7.63}(\text{Bi}_{7.57-8.19}\text{Sb}_{0.08-0.21})_{\Sigma 7.73-8.28}\text{S}_{20}$. Following the general formula for cosalite $(\text{Cu}_x\text{Ag}_y\text{Pb}_{8-2s-0.5(x+i)}\text{Bi}_{8+s}\text{S}_{20})$ proposed by Topa and Makovicky (2010), cosalite from Kizhnica is characterized by mainly $2(\text{Cu}^+ + \text{Ag}^+) \leftrightarrow \text{Pb}^{2+}$ substitution, where parameter *x* (the content of Cu) is in the range from 0.87 up to 1.33 (Fig. 10a). Silver is partially involved in substitution with Cu, and parameter *i* is in the range from 0.01 up to 0.38. Additionally, substitution $\text{Ag}^+ + \text{Bi}^{3+} \leftrightarrow 2\text{Pb}^{2+}$ (“lillianite” type of substitution) is presented in a low degree – the content of silver (*s*) is in the range from 0.02 up to 0.26 *apfu* (Fig. 10b). The content of trivalent

elements (Bi+Sb+As) is close to the ideal number 8 *apfu* (in the range 7.73–8.28), showing limited substitution of Ag for Bi. The $\text{Sb}^{3+} \leftrightarrow \text{Bi}^{3+}$ substitution is not significant – the concentration of Sb is up to 0.21 *apfu* in cosalite from the Janjevo (Fig. 10c).

There are two generations of **bournonite** in the samples from Janjevo (Fig. 4). Bournonite I forms irregular inclusions up to 50 μm within galena I aggregate. The younger generation of bournonite II occurs as irregular aggregates within tetrahedrite grains (Fig. 6l). The chemical formula of bournonite is $\text{Pb}_{1.01-1.05}\text{Cu}_{1.03-1.06}(\text{Sb}_{0.61-0.85}\text{As}_{0.07-0.30})_{\Sigma 0.90-0.93}\text{S}_{\Sigma 2.91-3.10}$. Bournonite from Janjevo exhibits enrichment in As (bournonite-seligmannite solid solution). The BSE images reflect an outer rim that is the most As-rich (0.3 *apfu*) (Fig. 6l).

Gustavite is a rare sulfosalt in the Janjevo ores. It usually forms lath-like crystals intergrowing with aikinite and krupkaite (Fig. 11a). It is partially replaced by an unknown phase (AgCuBiS_3) and younger pearceite (Fig. 11d–e). Gustavite from Janjevo has an average calculated chemical $N = 3.9$ (from 3.84 up to 4.06), and the average value of parameter x of AgBi substitution is 0.90, which is in good agreement with the highly substituted member of lillianite–gustavite solid solution. Number N (order number for lillianite homologues) was calculated using the formulae $N = -1 + 1/(\text{Bi}_1 + \text{Pb}_1/2 - 1/2)$ and $x = (\text{mol } \%^N_{\text{AgBi}} L) * (N-2)/200$, where we must firstly normalize analyses via $\text{Ag} + \text{Pb} + \text{Bi} = 1$, proposed by Makovicky and Karup-Møller (1977). Simultaneously Cu and Fe contents should be ignored. The chemical formula of gustavite from Janjevo is $(\text{Ag}_{0.86-0.91}\text{Cu}_{0.09-0.21}\text{Pb}_{1.07-1.12}\text{Fe}_{0.01-0.04}\text{Bi}_{2.69-2.83})_{\Sigma 5}\text{S}_{\Sigma 5.73-6.01}$. The concentrations of Cu and Fe measured with microprobe were likely affected by associated tetrahedrite and chalcopyrite. Calculations of numbers N , where Cu was added to the Ag, gave the average number $N = 4.87$ and where Cu was subtracted by $\text{Cu}^+ + \text{Pb}^{2+} \leftrightarrow \text{Bi}^{3+} + \square$ substitution gave the average number $N = 3.36$. In both cases, N is away from the real known lillianite homologues (4 or 5.5).

Members of **pearceite–polybasite group** are observed in paragenesis with $\text{Cu–Bi} \pm \text{Ag} \pm \text{As}$ sulfosalts in the ore from Janjevo. They are represented by the As-members: **pearceite** and **cupropearceite**. They form irregular aggregates or grains overgrowing Bi sulfosalts and replace tetrahedrite group minerals (Fig. 11b–e). The size of the grains or aggregates is up to a few hundred μm . The general formula of the pearceite–polybasite group minerals is $[\text{M}_6\text{T}_2\text{S}_7][\text{Ag}_9\text{CuS}_4]$, where $M = \text{Ag}, \text{Cu}$, and $T = \text{As}, \text{Sb}$ (Bindi et al. 2007a, b). Minerals of this group have two pseudo-layer modules: a $[\text{M}_6\text{T}_2\text{S}_7]^{2-}$ A module layer and a $[\text{Ag}_9\text{CuS}_4]^{2+}$ B module layer (Bindi et al. 2007a). Pearceite–cupropearceite from Janjevo has variable Ag and Cu contents, with Ag varying between 11.37 and 13.21 *apfu* and Cu content between 2.81 and 4.65 *apfu*. Analy-

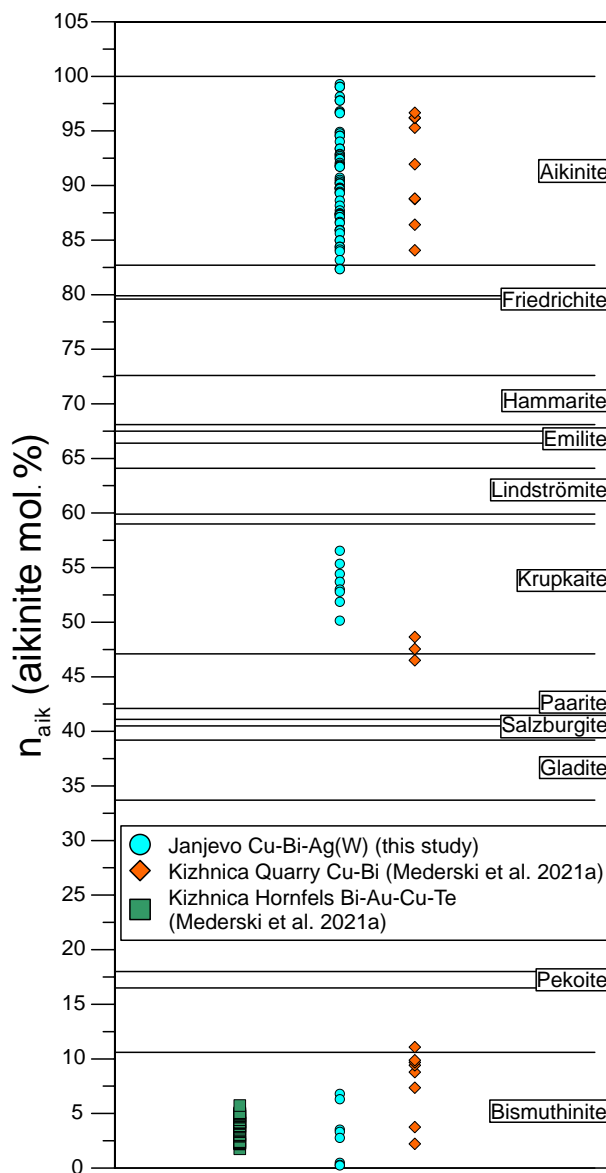


Fig. 8 – Position of the species of the bismuthinite–aikinite series from the Janjevo area determined by their n_{aik} after Topa et al. (2002).

ses that show a predominance of Cu (> 3 *apfu*) within the A module layer $[\text{M}_6\text{T}_2\text{S}_7]^{2-}$, represent the Cu-dominant member: cupropearceite (Fig. 12), according to the classification by Bindi et al. (2007a, b). Additionally, Sb content is neglectable, and the maximum content of Sb is 0.09 *apfu*. Pearceite is slightly enriched in Bi with maximum content of 0.19 *apfu*. These higher Bi concentrations are attributed to Bi-sulfosalts replaced by pearceite. Contents of other elements, such as Fe and Pb are low and reach a maximum of 0.04 *apfu* for Pb and 0.44 for Fe. The chemical formula for pearceite from Janjevo (based on sum of 18 cations) is $[(\text{Ag}_{2.99-4.21}\text{Cu}_{1.81-2.93}\text{Fe}_{0.09-0.44}\text{Pb}_{0.00-0.04})_{6.19-6.29}(\text{As}_{1.69-1.80}\text{Bi}_{0.01-0.04}\text{Sb}_{0.00-0.01})_{1.71-1.81}\text{S}_{6.69-7.04}][\text{Ag}_9\text{CuS}_4]$, while for cupropearceite is $[(\text{Ag}_{2.37-3.00}\text{Cu}_{3.08-3.65}$

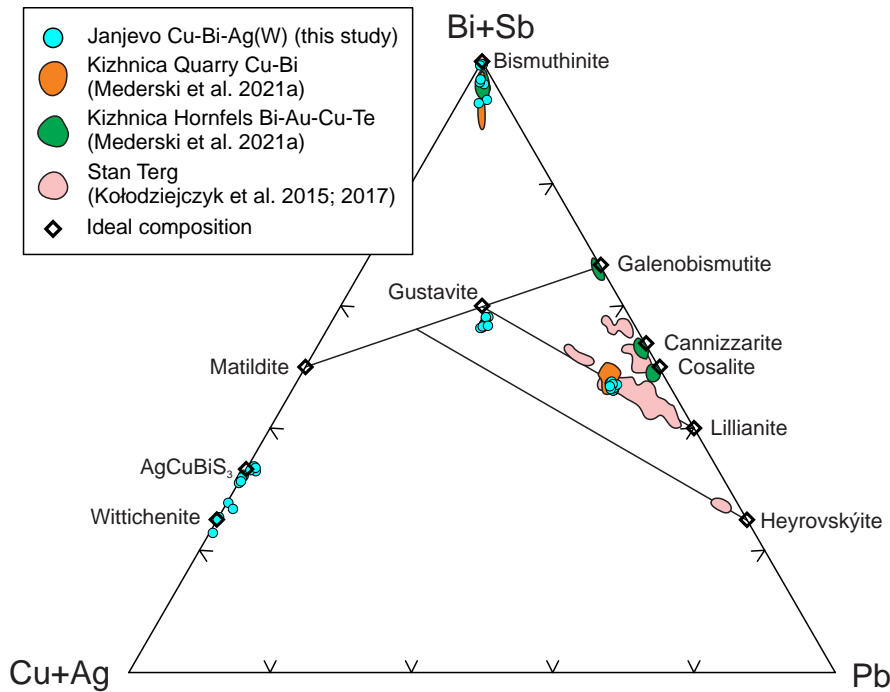
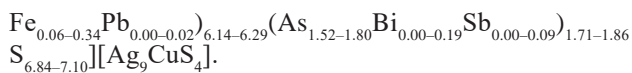
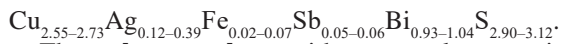


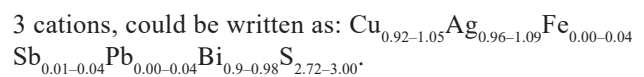
Fig. 9 – Ternary plot Cu+Ag vs. Bi+Sb vs. Pb of bismuth sulfosalts from the Janjevo, Kizhnica and the Stan Terg area (Kołodziejczyk et al. 2015, 2017; Mederski et al. 2021a).



Wittichenite is a rare phase at Janjevo. It occasionally occurs in small aggregates with other Bi sulfosalts – mainly aikinite and gustavite. The cation/anion ratio is 4 : 3, the same as in stoichiometric wittichenite composition. Chemically it is Ag – enriched and the content of Ag is up to 0.4 *apfu* (Tab. S3; Fig. 13). The formula of wittichenite calculated on the base of 4 cations could be written as:



The **unknown phase** with a general composition of **AgCuBiS₃** is very rare at the locality. It is associated with other Bi sulfosalts like aikinite, krupkaite, wittichenite, and gustavite, as well as with tetrahedrite and pearceite. It commonly occurs between older gustavite/aikinite and younger pearceite, forming aggregates up to 10 μm (Fig. 11d–e). Chemical composition is stable, including Ag, Cu, Bi, and S as the main elements (Tab. S3, ESM3; Fig. 13). The calculated cation/anion ratio is 3 : 3. This unknown phase could be compared with Cu-rich members of pavonite homologues. However, microprobe analyses have not detected Pb in sufficient concentrations, which is required for this group of minerals (Karup-Møller and Makovicky 1979; Močlo et al. 2008; Topa et al. 2012). The chemical composition of the unknown phase is close to Ag-rich wittichenite. However, the cation/anion ratio of the unknown phase 3 : 3 (or 4 : 4) does not match the 4 : 3 ratio in the theoretical wittichenite composition Cu₃BiS₃ (calculated on the base of 4 cations). The formula of the unknown phase, calculated on the base of



5.2.4. Other minerals

In addition, there is wolframite in the ore from Janjevo, which is represented by members of the **ferberite–hübnerite series**. Wolframite co-crystallized with quartz (Fig. 11f). It forms euhedral crystals up to 2 mm (Fig. 3f, 11g–h). Wolframite from Janjevo is characterized by a transitional chemical composition with variable Fe and Mn contents: $(\text{Fe}_{0.50-0.80} \text{Mn}_{0.23-0.54} \text{Ti}_{0.00-0.02} \text{Ca}_{0.00-0.02})_{\Sigma 1.03-1.07} [\text{WO}_4]_{0.97-0.99}$. Most of the chemical analyses plot in the classification field of ferberite, with only one analysis indicating hübnerite. Its position in the paragenetic sequence of Cu–Bi–Ag±W mineralization at Janjevo is not confirmed, and further studies are needed to determine the formation conditions. The potential epithermal origin of the Janjevo wolframite known from only a few locations in the world cannot be excluded (e.g., Kalinaj 1992; Milési et al. 1994; Bailly et al. 2002; Damian et al. 2016; Wagner et al. 2005; Skoupras et al. 2022).

Native bismuth is co-crystallized with arsenopyrite I and löllingite (Fig. 4). It occurs as irregular blebs up to 50 μm within aggregates of arsenopyrite I and löllingite (Fig. 5i–j). In addition, disseminated native bismuth crystals are observed within quartz and siderite. The analyzed droplets are chemically homogeneous, with small admixtures of Fe (up to 1.46 wt. %) and Sb (up to 0.32 wt. %), attributed to contamination of arsenopyrite and löllingite.

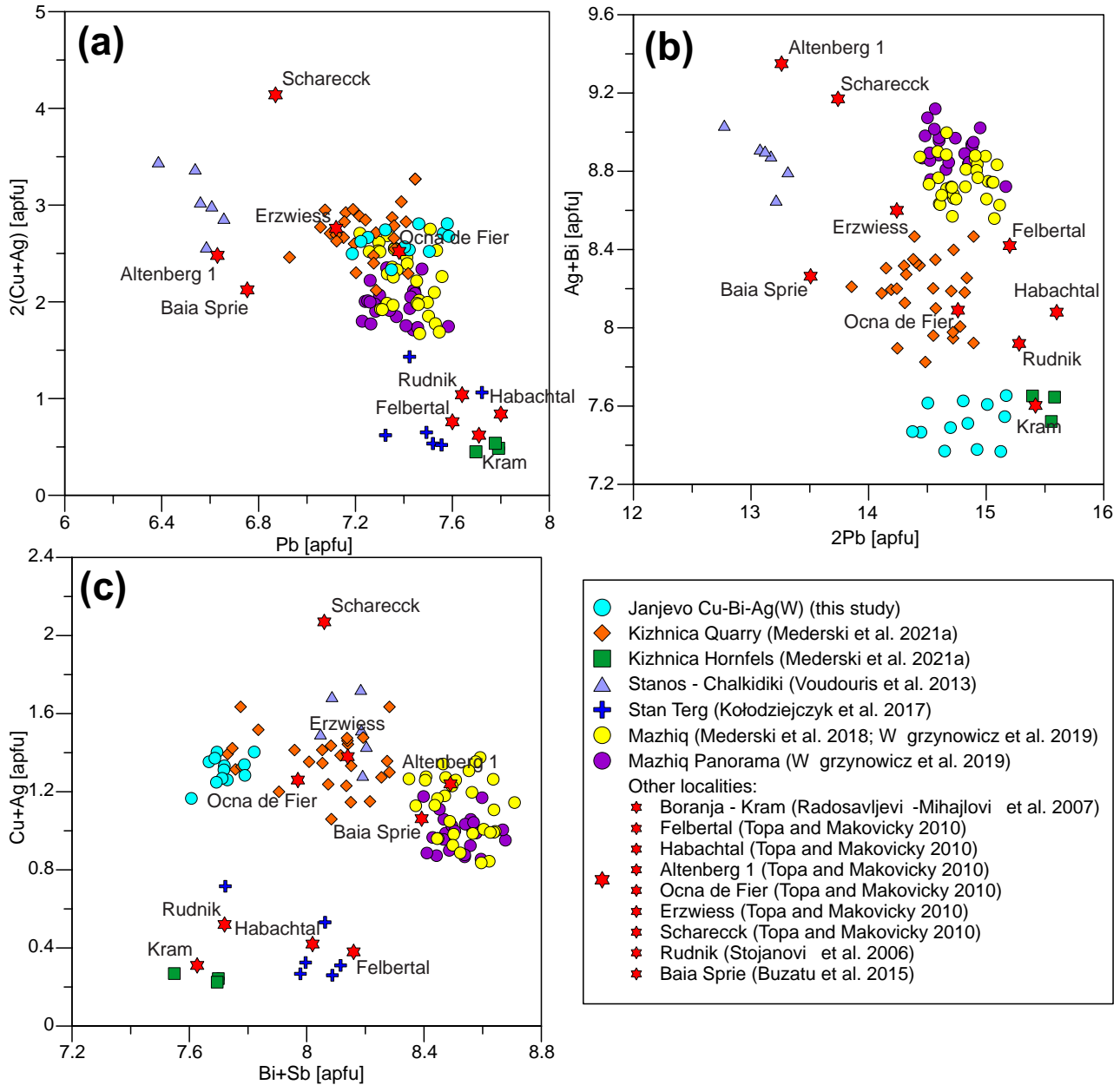


Fig. 10 – Binary plots showing the chemical composition of cosalite from the Janjevo area and known locations of cosalite from the literature (Stojanović et al. 2006; Radosavljević-Mihajlović et al. 2007; Topa and Makovicky 2010; Voudouris et al. 2013; Buzatu et al. 2015; Kołodziejczyk et al. 2017; Mederski et al. 2018, 2021a; Węgrzynowicz et al. 2019). **a** – 2(Cu+Ag) vs. Pb (apfu). **b** – Ag+Bi vs. 2Pb (apfu). **c** – Cu+Ag vs. Bi+Sb (apfu).

Siderite is the main component of the Janjevo veins. It crystallized during the early base metal stage, the main stage, and the late stage (Fig. 4). It forms coarse-crystalline aggregates with grains up to several cm (Fig. 3a–c). BSE images show oscillatory zonation (Fig. 11i), caused by variations in chemical composition, where Fe is being substituted not only by Mn, but also by Mg and Ca. The formula of siderite is $(\text{Fe}_{0.56-0.83}\text{Mn}_{0.14-0.38}\text{Mg}_{0.01-0.07}\text{Ca}_{0.00-0.03})_{\Sigma 1.00}\text{CO}_3$. Siderite from Janjevo was affected by weathering, with numerous cracks in the crystals or at the grain contacts, filled and replaced by Fe hydroxides (Fig. 11i).

Quartz is ubiquitous in the ore from Janjevo. It crystallized during all hydrothermal stages of precipitation (Fig. 4). It is the main vein-forming mineral of the bis-muth stage and co-crystallized with Bi sulfosalts (Fig. 3e; 6f–g, j–k).

5.3. Minor and trace elements in main ore minerals

Minor- and trace-elements analyses of pyrite, sphalerite, chalcopyrite, arsenopyrite, and tetrahedrite group miner-

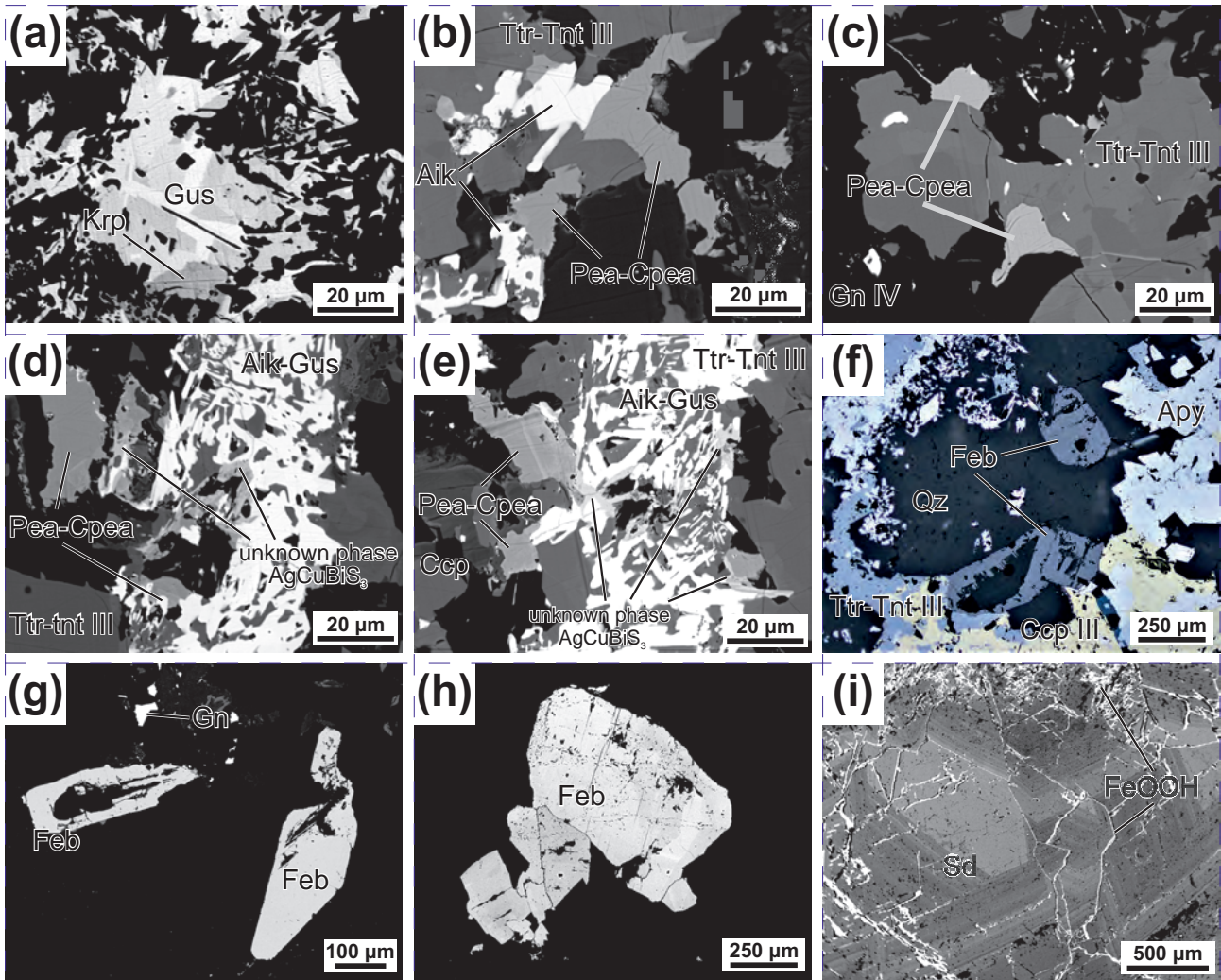


Fig. 11 – Reflected-light photomicrographs (f) and back-scattered electron (BSE) images (a–e, g–i) of Cu–Bi–Ag±W mineralization from the Janjevo. **a** – Gustavite–krupkaite aggregate. **b** – Pearceite–cupropearceite crystals associated with aikinite and tetrahedrite–tennantite. **c** – Pearceite–cupropearceite crystals associated with tetrahedrite–tennantite, and galena IV. **d** – Pearceite–cupropearceite crystals growing on older aikinite–gustavite aggregates and reaction rims with crystallized unknown phase AgCuBiS_3 . **e** – Reaction rings of unknown phase AgCuBiS_3 between pearceite–cupropearceite crystals and aikinite–gustavite aggregates, older tetrahedrite–tennantite–chalcopyrite aggregates. **f** – Euhedral wolframite (ferberite) crystals associated with quartz and tetrahedrite–tennantite–chalcopyrite III–arsenopyrite aggregates. **g** – Euhedral wolframite (ferberite) crystals, galena aggregates. **h** – Assemblages of euhedral wolframite (ferberite) crystals. **i** – Crystals of zonal siderite with supergene Fe hydroxides crystallized in cracks. AgCuBiS_3 – unknown phase AgCuBiS_3 , Aik – aikinite, Apy – arsenopyrite, Ccp – chalcopyrite, Cpea – cupropearceite, Feb – ferberite, FeOOH – Fe hydroxides, Gn – galena, Gus – gustavite, Krp – krupkaite, Pea – pearceite, Qz – quartz, Sd – siderite, Tnt – tennantite, Ttr – tetrahedrite.

als from Janjevo have been obtained from LA-ICP-MS and are presented in Tab. S4 (ESM 4). Additionally, Fig. 14 shows box plot diagrams of minor and trace elements in the studied minerals, where median, first quartile, third quartile, 5th percentile, 95th percentile, and outliers are indicated. The minerals mentioned above, which are sufficiently large and free of major inclusions and irregular intergrowths with other mineral phases, were used for studies using LA-ICP-MS. Therefore, minerals from the early base metal stage (pyrite and sphalerite I), bismuth stage (arsenopyrite I), and the main stage (sphalerite II, chalcopyrite III, arsenopyrite II, and

tetrahedrite group minerals) were selected for measurements. Representative time-resolved LA-ICP-MS depth profiles of studied ore minerals are presented in Fig. 15 and 16.

Pyrite is characterized by variable concentrations of As (up to 26,565 ppm, median: 14,769 ppm), significant contents of Ni (median: 662 ppm) and Co (median: 38.9 ppm) (Tab. S4). In addition, some analyses showed elevated concentrations of Au (up to 7.20 ppm, median: 2.27 ppm) and Te (up to 13.35 ppm).

In the ore from Janjevo, two generations of **sphalerite** are distinguished, which differ in their trace element con-

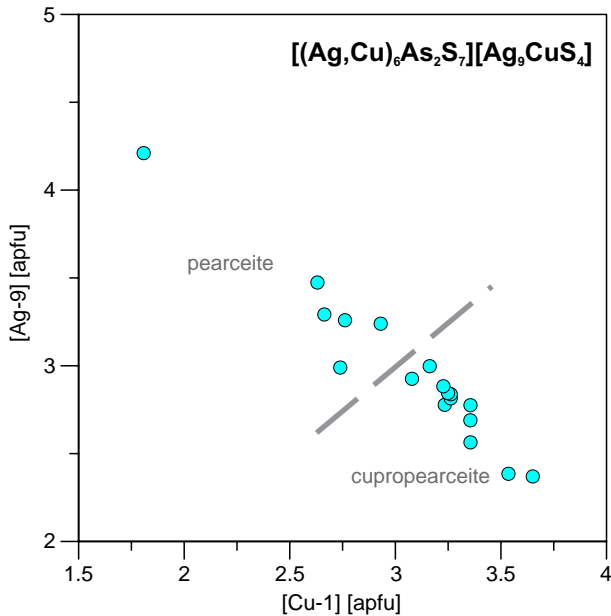


Fig. 12 – Cu-1 vs. Ag-9 binary plot (apfu) of pearceite–cupropearceite from the Janjevo (Bindi et al. 2007a).

tent. Sphalerite I is characterized by significantly higher Fe and Mn contents (medians: 29,817 ppm of Fe; 178 ppm of Mn), while sphalerite II contains 2,844 ppm Fe and 8.73 ppm Mn (medians). The medians of other trace elements in sphalerite are as follows and are higher for sphalerite I: Cu (I – 395 ppm, II – 387 ppm), In (I – 23.73 ppm, II – 3.05 ppm), Sn (I – 21.81 ppm, II – 6.07 ppm), Ga (I – 8.46 ppm, II – 6.77 ppm), Ge (I – 9.15 ppm, II – 3.9 ppm) (Tab. S4). On the other hand, higher Cd and Hg contents are observed in sphalerite II: for Cd (medians: I – 1,458 ppm, II – 2,782 ppm) and Hg (medians: I – 20.43 ppm, II – 38.39 ppm). Interestingly, only sphalerite II shows a signal of Bi (median 21.43 ppm), while the LA-ICP-MS spectrum show a homogeneous distribution (Fig. 15c).

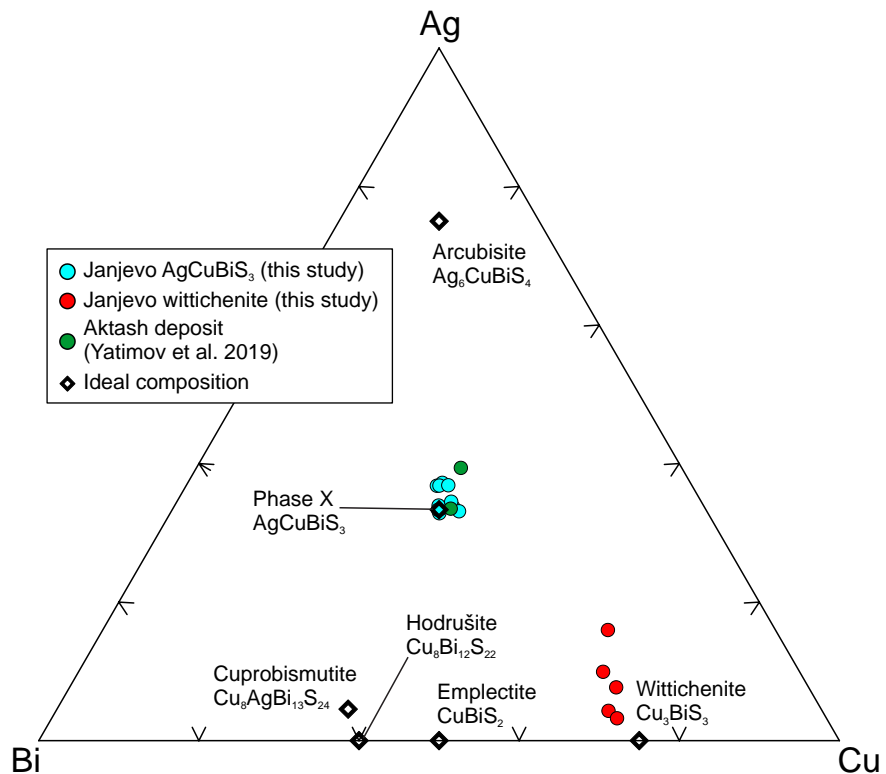
The main trace elements present in **chalcopyrite** III are Zn (median: 807 ppm), In (up to 142 ppm, median: 72.39 ppm), Sn (up to 158 ppm, median: 10.30 ppm), and Mn (median:

27.84 ppm) (Tab. S4; Fig. 15c). Tin and indium seem to be increased together in some zones (Fig 15d). The medians of other trace elements in chalcopyrite III are as follows: Cd (6.82 ppm), Ge (2.07 ppm), Ag (1.87 ppm), and Bi (1.42 ppm).

Antimony and bismuth are the main trace elements occurring in the structure of **arsenopyrite** from Janjevo. Arsenopyrite I is characterized by high concentrations of Sb (median: 15,483 ppm) and Bi (median: 3,383 ppm), while arsenopyrite II shows lower contents of Sb (median: 9,892 ppm) and Bi (median: 196 ppm) (Tab. S4). These elements in arsenopyrite I are incorporated either in the lattice of the mineral or in nano-inclusions, as suggested by the flat LA-ICP-MS spectra (Fig. 15e); moreover, analyses of arsenopyrite I were conducted on crystals without visible native Bi micro-inclusions (Fig. 6c). Other trace elements occurring in significant amounts are Cu (median: 603 ppm), and Pb (median: 455 ppm), which are the result of sulfide inclusions.

The **tetrahedrite group minerals** (TGM) can incorporate a wide range of major and trace elements. Minerals from this group occurring in the Janjevo ore form a solid solution with transitional chemistry from tetrahedrite to tennantite. For describing the trace elements, the population was divided into two groups: tetrahedrite and tennantite (Fig. 16a–c). Silver occurs in minor amounts in the TGM from Janjevo: the median Ag content in the tetrahedrite is 14,751 ppm and in the tennantite 940

Fig. 13 – Ternary plot Cu vs. Ag vs. Bi of unknown phase (AgCuBiS_3) and wittichenite from the Janjevo and Aktash deposits (Yatimov et al. 2019).



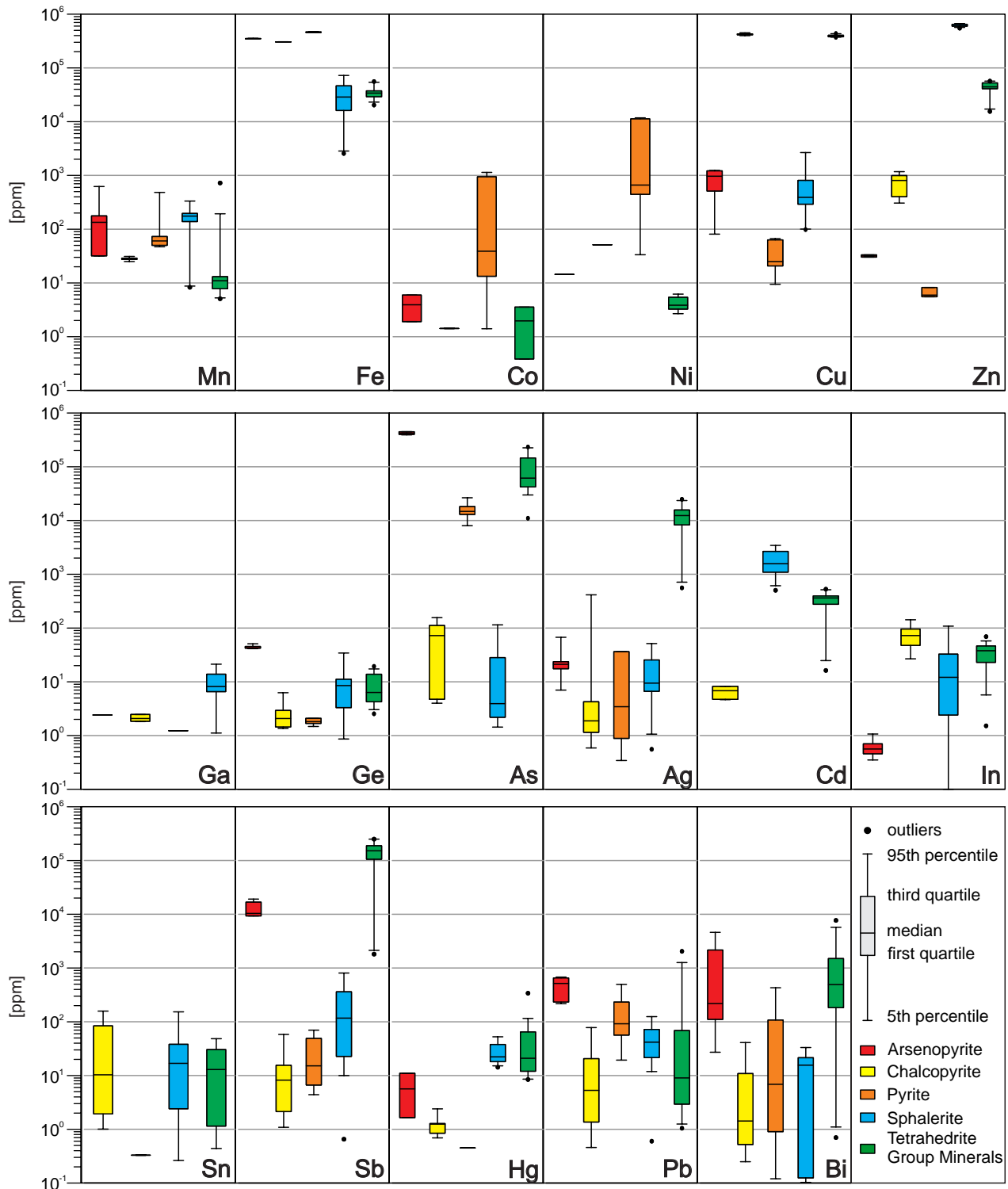


Fig. 14 – Box plot showing minor and trace element concentrations [in ppm] measured by LA-ICP-MS in arsenopyrite, chalcopyrite, pyrite, sphalerite, and tetrahedrite group minerals from the Janjevo Cu–Bi–Ag±W mineralization.

ppm. The medians of the divalent trace elements present at the C position in the tetrahedrite structure are: 371 ppm Cd, 16.40 ppm Hg, 11.54 Mn, and 5.25 ppm Pb.

The concentrations in tennantite are 65.5 ppm Cd, 57.33 ppm Hg, 8.84 ppm Mn, and 630 ppm Pb, respectively. The trivalent In medians are similar in both TGM, 38.95

ppm in tetrahedrite, and 36.69 ppm in tennantite. In addition, tennantite shows significantly higher Ge, Sn, and Tl concentrations (the medians are respectively 16.89 ppm, 30.33 ppm, and 5.8 ppm). In tetrahedrite the Ge concentrations are 5.21 ppm (median), while Sn and Tl are below the detection limit. Other trace element contents in TGM (Ga, Mo, Se, and Te) are in most of analyzed spots below detection limits.

6. Discussion

6.1. Sulfosalt mineral paragenesis and substitution trends

Bi–Pb±Cu±Ag and Cu–Bi±Ag±As sulfosalts are typically the primary carriers of Bi and Ag in the Cu–Bi zones of deeper hydrothermal deposits associated with volcanic rocks (Ciobanu and Cook 2000; Stojanović et al. 2006; Jeleň et al. 2012; Buzatu et al. 2015; Kołodziejczyk et al. 2015; Mederski et al. 2021a). There are two main sulfosalt parageneses in Janjevo: Bi–Pb±Cu±Ag and Cu–Bi±Ag±As paragenesis (Fig. 4). The first paragenesis is represented by bismuthinite, aikinite, krupkaite, cosalite, and gustavite, while the second includes pearceite, cupropearceite, wittichenite, and unknown phase: AgCuBiS_3 (Fig. 4).

The Bi–Pb±Cu±Ag paragenesis is relatively common in hydrothermal deposits from Vardar Zone (Stojanović et al. 2006, 2018; Radosavljević-

Mihajlović et al. 2007; Voudouris et al. 2008, 2013, 2018; Radosavljević et al. 2013; Budinov et al. 2015), especially in the Trepça Mineral Belt in Kosovo (Kołodziejczyk et al. 2015, 2017; Mederski et al. 2018, 2021a; Węgrzynowicz et al. 2019). The characteristic mineral of this paragenesis is cosalite, which, depending on genetic types of the mineralization and the nature of the fluids, shows considerable chemical variability. The substitutions observed in cosalite are: $2(\text{Cu}^+ + \text{Ag}^+) \leftrightarrow \text{Pb}^{2+}$ (Fig. 10a), $\text{Ag}^+ + \text{Bi}^{3+} \leftrightarrow 2\text{Pb}^{2+}$ “lillianite” type of substitution (Fig. 10b), or $\text{Sb}^{3+} \leftrightarrow \text{Bi}^{3+}$. A similar type of substitutions is observed in samples from Ocna de Fier

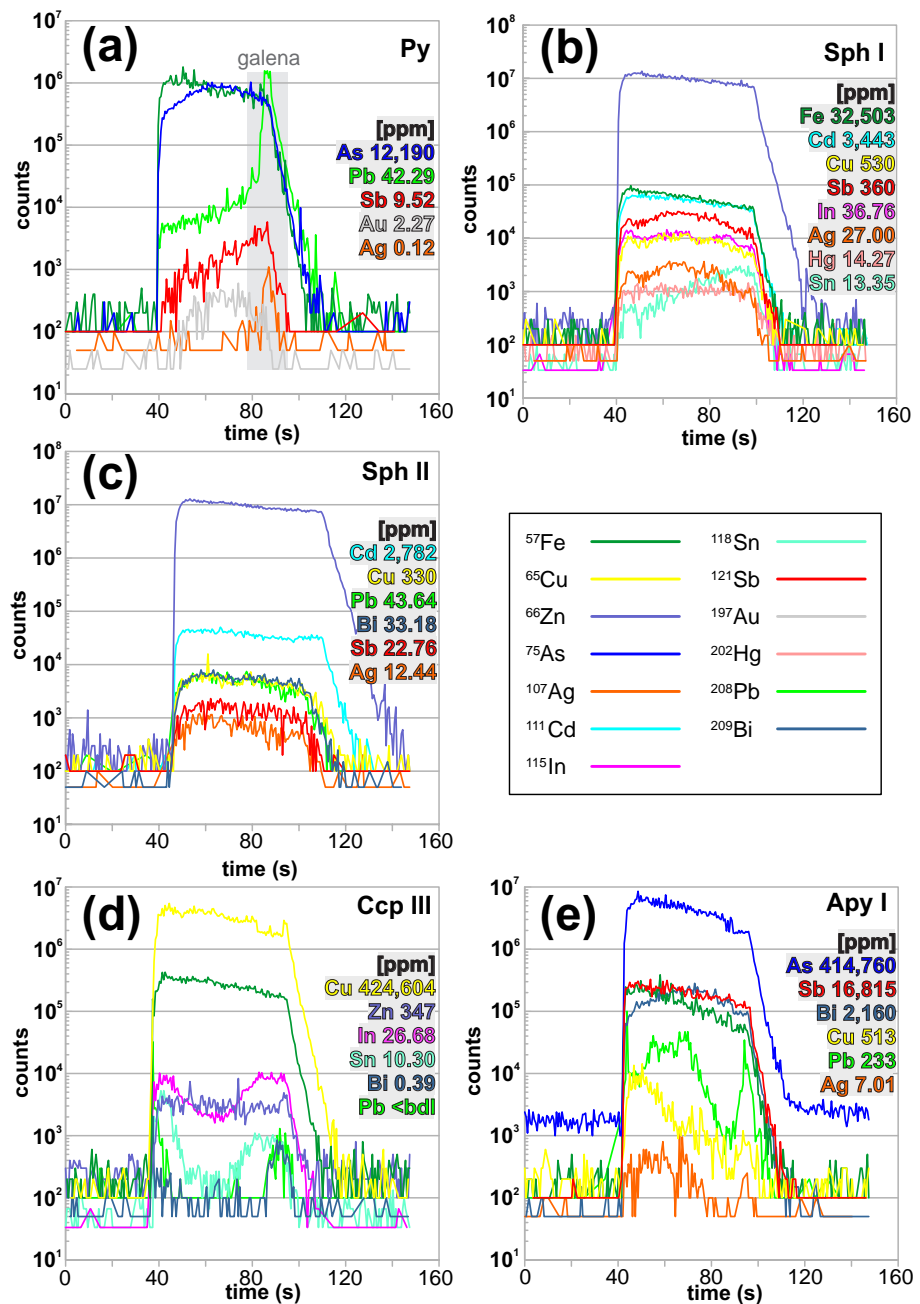


Fig. 15 – Representative time-resolved laser ablation ICP-MS depth profiles of sphalerite, chalcopyrite, and arsenopyrite from the Janjevo Cu–Bi–Ag±W mineralization. The contents of individual elements shown on the graphs refer to the specific measurement locations presented on the time-resolved laser ablation ICP-MS depth profiles (a–e). **a** – Pyrite. **b** – Sphalerite I. **c** – Sphalerite II. **d** – Chalcopyrite III with zones enriched in In and Sn. **e** – Arsenopyrite I.

Cu–Fe skarn (Topa and Makovicky 2010) and epithermal Cu–Bi veins in Trepča Mineral Belt: Kizhnica quarry and Mazhiq (Mederski et al. 2018, 2021a; Węgrzynowicz et al. 2019) (Fig. 10a–c). On the other hand, completely different trends are shown in cosalite from skarn localities known in the Serbo-Macedonian metallogenic province (Rudnik, Kram, Stan Terg, and Kizhnica hornfels) (Stojanović et al. 2006; Radosavljević-Mihajlović et al. 2007; Kołodziejczyk et al. 2017; Mederski et al. 2021a). In the Bi–Pb±Cu±Ag paragenesis, bismuthinite-aikinite series members are also very common, usually dominated by bismuthinite and krupkaite, while aikinite is an accessory mineral. On the other hand, in the Janjevo copper ore, aikinite is one of the main Bi sulfosalts. In addition, characteristic exsolutions of various members of the bismuthinite-aikinite series are absent from known locations in the Vardar Zone. Such exsolutions originate from primary phases, which crystallize at temperatures over 300 °C (Springer 1971) and are known from, e.g., the Ocna de Fier Cu–Fe skarn deposit (Ciobanu and Cook 2000) or the Felbertal W deposit (Topa et al. 2002, 2008).

Mineral paragenesis, in which Cu–Bi±Ag±As sulfosalts are the major minerals, is considerably rare. This paragenesis is commonly associated with intrusive magmatic rocks, including porphyry systems: hydrothermal veins (Jeleň et al. 2012; Izumino et al. 2014; Voudouris

et al. 2022), skarns (Ciobanu and Cook 2000; Ilinca 2006; Yatimov et al. 2019; Tămaş and Andrii 2020), and carbonate-replacements (Voudouris et al. 2008). It is typical for Cu–Bi±Ag±As paragenesis to be represented by complex mineralogy with sulfosalts, such as members of the cuprobismutite series and pavonite homologous series, emplectite, wittichenite, and occasionally pearceite, enargite, or luzonite. In the Janjevo occurrence, sulfosalts with Pb did not crystallize during the formation of the above paragenesis, because Pb was incorporated into Ag–Bi-rich galena at that stage. Relatively common in the Janjevo paragenesis are pearceite and cupropearceite. Pearceite is widespread in many hydrothermal deposits elsewhere in the world (e.g., Voudouris et al. 2022), while cupropearceite is rare and known only from a few locations (e.g., Bindi et al. 2007b, 2015; Bindi and Pekov 2009; Sejkora et al. 2010; Kozub-Budzyń and Piestrzyński 2018). However, we observe a continuous variation in Ag and Cu concentrations on the A module layer $[M_6T_2S_7]^2$ in pearceite–cupropearceite members from Janjevo, while both members in one paragenesis in the world are rare. Experimental studies by Harlov and Sack (1994) indicate that the widest Cu–Ag substitutional range is observed in the temperatures 75 °C and 150 °C, which is similar to data from Janjevo, where we observe a variation in Cu content from 8.5 to 14.5

wt. %. Another unique mineral in Janjevo is the unknown phase – AgCuBiS₃. It was formed in reaction zones between pearceite–cupropearceite and older gustavite/ aikinite aggregates. A mineral of similar chemical composition is described in the Aktash deposit by Yatimov et al. (2019). Yatimov et al. (2019) identified this phase as Ag-bearing wittichenite, and it occurs in a paragenesis similar to Janjevo – members of the bismuthinite–aikinite series, wittichenite, emplectite, and galenobismutite. Recalculating the chemical analyses of this

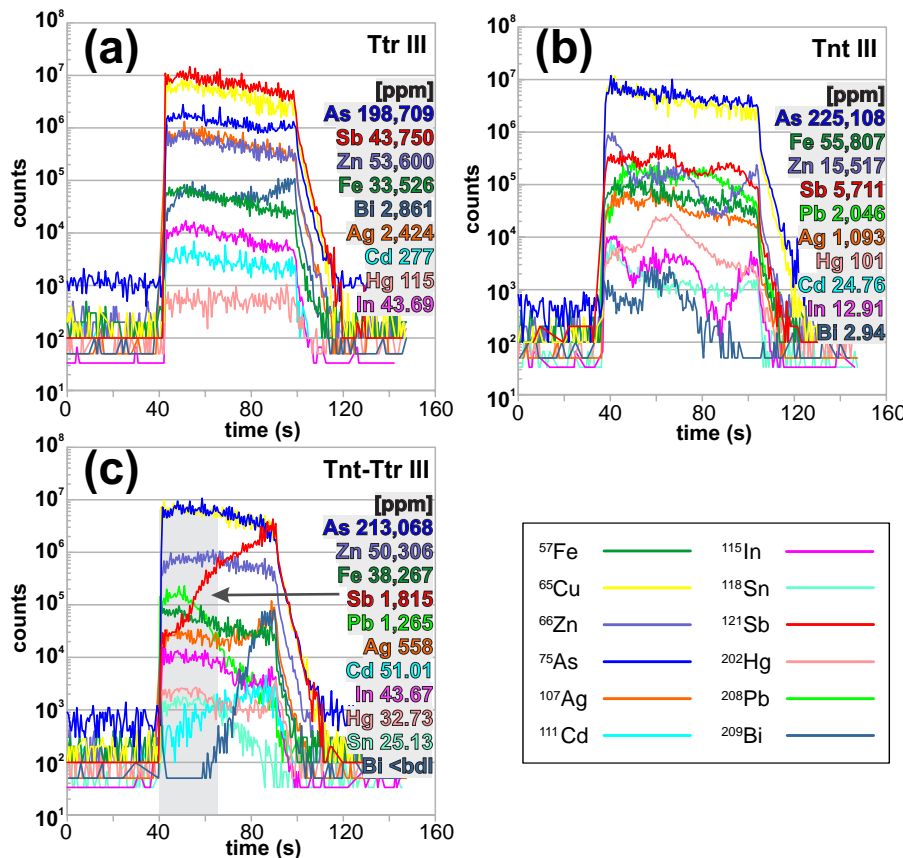


Fig. 16 – Representative time-resolved laser ablation ICP-MS depth profiles of tetrahedrite group minerals from the Janjevo Cu–Bi–Ag±W mineralization. The contents of individual elements shown on the graphs refer to the specific measurement locations presented on the time-resolved laser ablation ICP-MS depth profiles (a–c). **a** – Tetrahedrite III. **b** – Tennantite III. **c** – A transition zone between tennantite III and tetrahedrite III.

mineral from Aktash based on 3 cations gives the following empirical formula: $\text{Cu}_{0.99-1.01}\text{Ag}_{0.98-1.18}\text{Fe}_{0.00-0.08}\text{Bi}_{0.83-0.93}\text{S}_{2.85-3.00}$, which is close to the empirical formula of the unknown phase AgCuBiS_3 from Janjevo. In addition, the compilation of data from Aktash and Janjevo in a ternary plot Cu vs. Ag vs. Bi indicates a similar chemical composition and highlights a high homogeneity of the AgCuBiS_3 mineral from Janjevo (Fig. 13).

6.2. Trace elements distribution

The complexity of the Cu–Bi–Ag±W mineralization from Janjevo, in addition to the presence of many sulfosalts, is manifested by the presence of several generations of base metal sulfides (BMS), which could be distinguished due to textural features as well as trace elements (Fig. 4). Trace elements from the order of a few ppm to tens of thousands of ppm were measured by laser ablation inductively-coupled plasma mass spectrometry (LA-ICP-MS). The method is widely applicable to many ore minerals from various genetic types and many studies have been published over the past 20 years: sphalerite (e.g., Cook et al. 2009; Frenzel et al. 2016), pyrite (e.g., Large et al. 2009; Wang et al. 2021), chalcopyrite (e.g., George et al. 2018; Foltyn et al. 2022), and arsenopyrite (e.g., Lee et al. 2019; Gourcerol et al. 2020). However, despite the widespread occurrence of tetrahedrite group minerals (TGM) in hydrothermal environments, only a few works address the issue of trace elements in TGM (George et al. 2017; Sitarz et al. 2021; Silyanov et al. 2022). Moreover, studies of the partitioning of trace elements in sphalerite + galena + chalcopyrite (± tetrahedrite group minerals) in hydrothermal ores indicate preferential trends of individual trace elements and potential co-crystallization (George et al. 2016, 2017). Observation of the time-resolved downhole ablation profiles (Fig. 15a–e; 16a–c) helps distinguish obvious micro-inclusions in the host mineral (Cook et al. 2016). Furthermore, the steadiness of LA-ICP-MS profiles may be related to trace elements as solid solutions or the occurrence of homogeneously distributed nano-inclusions.

Bismuth in the Cu–Bi–Ag±W ore from Janjevo occurs in the form of numerous sulfosalts, but its significant concentrations are also found in ore minerals measured by the LA-ICP-MS technique. Very high Bi contents of up to 4,600 ppm exhibit arsenopyrite I, which is widely distributed in the ore. By crystallization of arsenopyrite I begins the productive stage for bismuth (stage 2) (Fig. 4), where the ore shows textures of decomposition and crystallization of native Bi inside arsenopyrite I–löllingite aggregates (Fig. 5i–j). In addition, crystallization of Bi sulfosalts in Janjevo took place after the formation of arsenopyrite I (Fig. 4). The incorporation of bismuth into BMS differs depending on the generation of individual

sulfides (Fig. 14). In general, the bismuth among BMS is preferentially incorporated into galena co-crystallizing with other sulfides (George et al. 2015, 2016). Bismuth measured by microprobe in galena IV ranged up to 9.27 wt. %, and in galena II, up to 2 wt. %. Significantly less Bi is found in the other minerals analyzed, where the medians are: 565 ppm for tetrahedrite III, 2.94 ppm for tennantite, 196 ppm for arsenopyrite II, 1.42 ppm for chalcopyrite III, and 21.43 ppm for sphalerite II. The mild enrichment in Bi in sphalerite II seems unusual, especially since the LA-ICP-MS spectrum is flat. The incorporation of bismuth into the sphalerite structure is unknown in the literature (Cook et al. 2009). The flat LA-ICP-MS spectrum and the high abundance of Bi-minerals in the whole paragenesis suggest rather the presence of homogeneously distributed micro- to nano-inclusion of Bi sulfosalts. Similar patterns are observed for Cu, Pb, Sb, and Ag so that they can be linked to the nano-inclusions of sulfosalts together with Bi (Fig. 15b). Elevated Bi content in sphalerite associated with micro-inclusions is reported from some metamorphosed sulfide deposits (Lockington et al. 2014).

Indium is another significant trace element that is present in the entirety of the Kizhnica–Hajvalia–Badovc ore field, as well as in Cu–Bi–Ag±W mineralization from Janjevo (Mederski et al. 2022b). Indium is a critical metal and the ores from the Kizhnica–Badovc area (epithermal veins and listvenite ores) show considerable economic potential in the context of elevated indium contents. Indium shows lower concentrations in ore minerals from Janjevo compared to other occurrences nearby. However, the geochemical importance of this element is still well visible. The main mineral hosting indium in ores from Kizhnica–Badovc is sphalerite (Mederski et al. 2019, 2021a, b), which reaches In concentrations up to several thousand ppm (3,160 ppm in sphalerite from listvenites and 1,600 ppm in sphalerite from Cu–Bi veinlets in Kizhnica quarry). Interestingly, sphalerite in Janjevo is not the main mineral hosting indium. Sphalerite I reaches values up to 108 ppm (median: 23.73 ppm), while sphalerite II contains up to 12.09 ppm In (median: 3.05 ppm). Higher concentrations of In are found in phases co-crystallizing with sphalerite II: chalcopyrite III (median: 72.39 ppm) and tetrahedrite–tennantite III (median: 38.94 ppm for tetrahedrite, and 36.68 ppm for tennantite). Previous studies show that, among the other base ore minerals, sphalerite is the most preferred mineral to incorporate In into the structure (George et al. 2016, 2017). The presence of indium in sphalerite and chalcopyrite is known in many genetic types of deposits (e.g., Murakami and Ishihara 2013; Foltyn et al. 2020; Xu et al. 2021; Voudouris et al. 2022), while the presence of this element in tetrahedrite group minerals is little documented (George et al. 2017). So far, elevated indium concentrations in tetrahedrite

group minerals have been reported only in two In-rich deposits: Neves Corvo (Portugal) – 0.15–2.7 wt. % (Gaspar 2002; Carvalho et al. 2018), and Pefka (Greece) – 4.03–6.5 wt. % (Voudouris et al. 2022). High indium contents are associated with the tennantite series in these deposits. In the studied tetrahedrite group minerals from Janjevo, indium concentrations do not depend on As-Sb substitution and reach similar contents of ~38 ppm.

Sphalerite is the main carrier of such trace elements as Cd, Hg, Ga, and Ge in the Cu–Bi–Ag±W ore from Janjevo (Fig. 14). The concentrations of Ga, Ge, with In, Fe, and Mn can be used to estimate crystallization temperatures using GGIMFis geothermometry (Ga, Ge, In, Mn and Fe in sphalerite) proposed by Frenzel et al. (2016). Sphalerite I from Janjevo crystallized at 220–272 °C, while sphalerite II precipitated at a much lower temperature: 160–190 °C (Tab. S4, ESM 4). The crystallization temperatures of the younger sphalerite generation correspond to the conditions responsible for the formation of the main-stage mineralization, which is typical of low-temperature, epithermal systems (i.e., Cu–Bi±Ag±As sulfosalts). In general, the formation temperatures of sphalerite at Janjevo coincide with those of sphalerite formation from other styles of mineralization in the Kizhnica–Hajvalia–Badovc ore field: Kizhnica quarry Cu–Bi epithermal veinlets (250–270 °C), Janjevo polymetallic veinlets (~340 °C), Janjevo Sb–As–Tl–Hg sediment-hosted mineralization (230–260 °C), Badovc Pb–Zn–Sb(Ni) listvenite hosted (210–380 °C), Badovc Pb–Zn–Sb banded vein-type (250–330 °C), and Badovc Sb vein-type (180–240 °C) (Mederski et al. 2022b). The geochemistry of sphalerite reflects the zonation within the KHB ore field: low-Fe sphalerite, including that from the study site, is observed within the Bi–Cu±Au zone (eastern part), while high-Fe sphalerite is mainly observed within the Pb–Zn–Sb±Ni zone (central and western part) (Mederski et al. 2022b).

7. Conclusions

A new type of Bi–Cu±Au mineralization was identified in the Kizhnica–Hajvalia–Badovc ore field in Vardar Zone – hydrothermal Cu–Bi–Ag±W mineralization in Janjevo. Bismuth sulfosalts are an important component in Bi–Cu±Au mineralization. Whereas the Bi–Pb±Cu±Ag sulfosalts paragenesis is widely known in many deposits in the Vardar Zone, the Cu–Bi±Ag±As paragenesis is described in Kosovo and this part of the Vardar Zone for the first time.

Our studies show that in addition to numerous Bi sulfosalts in Janjevo ores, bismuth has been incorporated into base metal sulfides and arsenopyrite. In particular, the main carrier of bismuth is arsenopyrite I, which has started the crystallization of the bismuth stage.

The application of GGIMFis geothermometry (Frenzel et al. 2016) on sphalerite from Cu–Bi–Ag±W ore from Janjevo gives the following sphalerite precipitation temperatures: 220–272 °C for sphalerite I and 160–190 °C for sphalerite II, consistent with the ore textures indicative of the polyphasic development of the mineralization.

Acknowledgments. The research was funded by Society of Economic Geologists Canada Foundation (SEGCF) Student Research Grant 2019 and by AGH statutory grant no. 16.16.140.315. We are grateful to Tomáš Mikuš, Gheorghe Damian, and the anonymous reviewer for comments and suggestions that helped significantly improve the manuscript. Handling Editor Jiří Sejkora is also thanked for his efficient handling of the manuscript. We are grateful to Adam Włodek and Gabriela Kozub-Budzyń from the Laboratory of Critical Elements at AGH-UST, Faculty of Geology, Geophysics and Environmental Protection, for their help during EMPA data collection. In addition, I would like to thank the many AGH students for their help in the fieldworks. Special thanks for their significant contribution to the fieldwork goes to Konrad Pytel.

Electronic supplementary material. Complete data for electron-probe microanalyses of minerals and LA-ICP-MS data from Janjevo are available online at the Journal website (<http://dx.doi.org/10.3190/jgeosci.371>).

References

- BAILLY L, GRANCEA L, KOUZMANOV K (2002) Infrared microthermometry and chemistry of wolframite from the Baia Sprie epithermal deposit, Romania. *Econ Geol* 97: 415–423
- BAKER T (2019) Gold±copper endowment and deposit diversity in the Western Tethyan Magmatic Belt, Southeast Europe: Implications for exploration. *Econ Geol* 114: 1237–1250
- BIAGIONI C, GEORGE LL, COOK NJ, MAKOVICKY E, MOËLO Y, PASERO M, SEJKORA J, STANLEY CJ, WELCH MD, BOSI F (2020) The tetrahedrite group: Nomenclature and classification. *Amer Miner* 105: 109–122
- BINDI L, PEKOV IV (2009) Crystal chemistry of extremely Cu-rich cupropearceite from the Sarbay mine, Northern Kazakhstan. *Zap Vsesoyuz Mineral Obshch* 138: 44–44
- BINDI L, EVAÏN M, SPRY PG, TAIT KT, MENCHETTI S (2007a) Structural role of copper in the minerals of the pearceite-polybasite group: The case of the new minerals cupropearceite and cupropolybasite. *Mineral Mag* 71: 641–650
- BINDI L, EVAÏN M, SPRY PG, MENCHETTI S (2007b) The pearceite-polybasite group of minerals: Crystal chemistry and new nomenclature rules. *Amer Miner* 92: 918–925

- BINDI L, TOPA D, KEUTSCH FN (2015) How much copper can the pearceite structure sustain? The case of cupropearceite from Tsumeb, Namibia. *Period Mineral* 84: 341–350
- BOROJEVIĆ ŠOŠTARIĆ S, PALINKAŠ LA, TOPA D, SPANGENBERG, JE, PROCHASKA W (2011) Silver-base metal epithermal vein and listwaenite types of deposit Crnac, Rogozna Mts., Kosovo. Part I: Ore mineral geochemistry and sulfur isotope study. *Ore Geol Rev* 40: 65–80
- BOROJEVIĆ ŠOŠTARIĆ S, CVETKOVIĆ V, NEUBAUER F, PALINKAŠ, LA, BERNROIDER M, GENSER J (2012) Oligocene shoshonitic rocks of the Rogozna Mts. (Central Balkan Peninsula): Evidence of petrogenetic links to the formation of Pb–Zn–Ag ore deposits. *Lithos* 148: 176–195
- BOROJEVIĆ ŠOŠTARIĆ S, PALINKAŠ LA, NEUBAUER F, HURAI V, CVETKOVIĆ V, ROLLER-LUTZ Z, MANDIĆ M AND GENSER J (2013) Silver-base metal epithermal vein and listwanite hosted deposit Crnac, Rogozna Mts., Kosovo, part II: A link between magmatic rocks and epithermal mineralization. *Ore Geol Rev* 50: 98–117
- BUDINOV ZD, YONEZU K, TINDELL T, GABO-RATIO JA, MILUTINOVIC S, BOYCE AJ, WATANABE K (2015) Copper-gold skarn mineralization at the Karavansalija ore zone, Rogozna Mountain, Southwestern Serbia. *Resour Geol* 65: 328–344
- BUERGER R, GIROUX G (2016) Technical report on the Slivovo gold–silver project. *Avrupa-Minerals*, Pristina, Kosovo, pp 1–108
- BUZATU A, DAMIAN G, DILL HG, BUZGAR N, APOPEI AI (2015) Mineralogy and geochemistry of sulfosalts from Baia Sprie ore deposit (Romania) – New bismuth minerals occurrence. *Ore Geol Rev* 65: 132–147
- CARVALHO JRS, RELVAS JMRS, PINTO AMM, FRENZEL, M, KRAUSE J, GUTZMER J, PACHECO N, FONSECA R, SANTOS S, CAETANO P, REIS T, GONÇALVES M (2018) Indium and selenium distribution in the Neves-Corvo deposit, Iberian Pyrite Belt, Portugal. *Mineral Mag* 82: 5–41
- CIOBANU CL, COOK NJ (2000) Intergrowths of bismuth sulphosalts from the Ocna de Fier Fe-skarn deposit, Banat, Southwest Romania. *Eur J Mineral* 12: 899–917
- COOK NJ, CIOBANU CL, PRING A, SKINNER W, SHIMIZU M, DANYUSHEVSKY L, SAINI-EIDUKAT B, MELCHER F (2009) Trace and minor elements in sphalerite: A LA-ICPMS study. *Geochim Cosmochim Acta* 73: 4761–4791
- COOK N, CIOBANU C, GEORGE L, ZHU Z-Y, WADE B, EHRIG K (2016) Trace element analysis of minerals in magmatic–hydrothermal ores by laser ablation inductively-coupled plasma mass spectrometry: Approaches and opportunities. *Minerals* 6: 111
- CVETKOVIĆ V, PRELEVIĆ D, DOWNES H, JOVANOVIĆ M, VASELLI O, PÉCSKAY Z (2004) Origin and geodynamic significance of Tertiary postcollisional basaltic magmatism in Serbia (central Balkan Peninsula). *Lithos* 73: 161–186
- DAMIAN G, DAMIAN F, KOLLÁROVÁ V, KONEČNY P (2016) A new occurrence of wolframite–ferberite in Romania. *Roman J Mineral Deposits* 89: 49–54
- DANGIĆ A (1985) Minor element distribution between galena and sphalerite as a geothermometer – application to two lead-zinc areas in Yugoslavia. *Econ Geol* 80: 180–183
- ELEZAJ Z (2009) Geodynamic evolution of Kosovo during the Triassic and Jurassic. *Yerbilimleri* 30: 113–126
- FOLTYN K, BERTRANDSSON ERLANDSSON V, KOZUB-BUDZYŃ GA, MELCHER F, PIETRZYŃSKI A (2020) Indium in polymetallic mineralisation at the Gierczyn mine, Karakonosze–Izera Massif, Poland: results of EPMA and LA-ICP-MS investigations. *Geol Q* 64: 74–85
- FOLTYN K, BERTRANDSSON ERLANDSSON V, ZYGO W, MELCHER F, PIECZONKA J (2022) New perspective on trace element (Re, Ge, Ag) hosts in the Cu–Ag Kupferschiefer deposit, Poland: Insight from a LA-ICP-MS trace element study. *Ore Geol Rev* 143: 104768
- FRENZEL M, HIRSCH T, GUTZMER J (2016) Gallium, germanium, indium, and other trace and minor elements in sphalerite as a function of deposit type – A meta-analysis. *Ore Geol Rev* 76: 52–78
- GASPAR OC (2002) Mineralogy and sulfide mineral chemistry of the Neves-Corvo ores, Portugal: insight into their genesis. *Canad Mineral* 40: 611–636
- GEORGE L, COOK NJ, CIOBANU CL, WADE BP (2015) Trace and minor elements in galena: A reconnaissance LA-ICP-MS study. *Amer Miner* 100: 548–569
- GEORGE LL, COOK NJ, CIOBANU CL (2016) Partitioning of trace elements in co-crystallized sphalerite–galena–chalcopyrite hydrothermal ores. *Ore Geol Rev* 77: 97–116
- GEORGE LL, COOK NJ, CIOBANU CL (2017) Minor and trace elements in natural tetrahedrite–tennantite: Effects on element partitioning among base metal sulphides. *Minerals* 7: 17
- GEORGE LL, COOK NJ, CROWE BBP, CIOBANU CL (2018) Trace elements in hydrothermal chalcopyrite. *Mineral Mag* 82: 59–88
- GOURCEROL B, KONTAK DJ, PETRUS JA, THURSTON PC (2020) Application of LA-ICP-MS analysis of arsenopyrite to gold metallogeny of the Meguma Terrane, Nova Scotia, Canada. *Gondwana Res* 81: 265–290
- GUILLONG M, MEIER DL, ALLAN MM, HEINRICH CA, YARDLEY BW (2008) Appendix A6: SILLS: A MATLAB-based program for the reduction of laser ablation ICP-MS data of homogeneous materials and inclusions. *Mineral Assoc Canada, Short Course* 40: 328–333
- HARLOV DE, SACK RO (1994) Thermochemistry of polybasite–pearceite solid solutions. *Geochim Cosmochim Acta* 58: 4363–4375
- HYSANI S, DURMISHAJ B, FETAHAJ B, SHALA F, BERISHA A, LARGE D (2010) Trepça Ore Belt and Stan Terg mine – Geological overview and interpretation, Kosovo (SE Europe). *Geologija* 53: 87–92

- ILINCA G (2006) Rare sulphosalts minerals in Romania. *Acta Mineral Petrogr*, Ser 5: 42–46
- IZUMINO Y, NAKASHIMA K, NAGASHIMA M (2014) Cuprobismutite group minerals (cuprobismutite, hodrušhite, kupčikite and paděraite), other Bi-sulfosalts and Bi-tellurides from the Obari mine, Yamagata Prefecture, Japan. *J Mineral Petrol Sci* 109: 177–190
- JANKOVIĆ S (1995) The principal metallogenic features of the Kopaonik District. In: *Geology and metallogeny of the Kopaonik Mt. Symposium*. pp 79–101
- JANKOVIĆ S (1997) The Carpatho-Balkanides and adjacent area: a sector of the Tethyan Eurasian metallogenic belt. *Miner Depos* 32: 426–433
- JELEŇ S, PRŠEK J, KOVALENKER VA, TOPA D, SEJKORA J, ŠTEVKO M, OZDÍN D (2012) Bismuth sulfosalts of the cuprobismutite, pavonite and aikinite series from the Rozália mine, Hodruša–Hámre, Slovakia. *Canad Mineral* 50: 325–340
- KALINAJ M (1992) Ferberite – a new mineral in the Štiavnica–Hodruša ore field. *Miner Slov* 24: 471–475 (in Slovak)
- KARUP-MØLLER S, MAKOVICKY E (1979) On pavonite, cupropavonite, benjaminite and “oversubstituted” gustavite. *Bull Mineral Petrol* 102: 351–367
- KOŁODZIEJCZYK J, PRŠEK J, MELFOS V, VOUDOURIS, PC, MALIQI F, KOZUB-BUDZYŃ G (2015) Bismuth minerals from the Stan Terg deposit (Trepča, Kosovo). *Neu Jb Mineral, Abh* 192: 317–333
- KOŁODZIEJCZYK J, PRŠEK J, VOUDOURIS PC, MELFOS V, ASLLANI B (2016a) Sn-bearing minerals and associated sphalerite from lead–zinc deposits, Kosovo: An electron microprobe and LA-ICP-MS study. *Minerals* 6: 42
- KOŁODZIEJCZYK J, PRŠEK J, ASLLANI B, MALIQI F (2016b) The paragenesis of silver minerals in the Pb–Zn Stan Terg deposit, Kosovo – an example of precious metal epithermal mineralization. *Geol Geophys Environ* 42: 19–29
- KOŁODZIEJCZYK J, PRŠEK J, VOUDOURIS PC, MELFOS V (2017) Bi-sulphotellurides associated with Pb–Bi–(Sb±Ag,Cu,Fe) sulphosalts: an example from the Stan Terg deposit in Kosovo. *Geol Carpath* 68: 366–381
- KOZUB-BUDZYŃ GA, PIETRZYŃSKI A (2018) The first occurrence of cupropearceite in the Kupferschiefer deposit, Lubin mine, SW Poland. *Geol Q* 62: 319–326
- LARGE RR, DANYUSHEVSKY L, HOLLIT C, MASLENNIKOV V, MEFFRE S, GILBERT S, BULL S, SCOTT R, EMSBO P, THOMAS H, SINGH B, FOSTER J (2009) Gold and trace element zonation in pyrite using a laser imaging technique: Implications for the timing of gold in orogenic and Carlin-style sediment-hosted deposits. *Econ Geol* 104: 635–668
- LEE M, SHIN D, YOO B, IM H, PAK S, CHOI S (2019) LA-ICP-MS trace element analysis of arsenopyrite from the Samgwang gold deposit, South Korea, and its genetic implications. *Ore Geol Rev* 114: 103147
- LOCKINGTON JA, COOK NJ, CIOBANU CL (2014) Trace and minor elements in sphalerite from metamorphosed sulphide deposits. *Mineral Petrol* 108: 873–890
- MAKOVICKY E, KARUP-MØLLER S (1977) Chemistry and crystallography of the lillianite homologous series. I. General properties and definitions. *Neu Jb Mineral, Abh* 130: 264–287
- MEDERSKI S, PRŠEK J, ASLLANI B, KOZUB-BUDZYŃ G (2018) Bi-sulphosalts from the Mazhiq, Stan Terg area, Kosovo. In: *Proceedings of the 5th Central-European Mineralogical Conference and 7th Mineral Sciences in the Carpathians Conference*. Banska Štiavnica, Slovakia, pp 74
- MEDERSKI S, PRŠEK J, HINCYNIGIER K (2019) Pb–Zn–Sb–Ni–Au mineralization from the Kizhnica area, central Kosovo: new data on the listwaenite type mineralization. In: *Proceedings of the Life with Ore Deposits on Earth: 15th Biennial SGA Meeting*. University of Glasgow Publicity Services, Glasgow, Scotland, pp 834–837
- MEDERSKI S, PRŠEK J, DIMITROVA D, HYSENI B (2021a) A combined EPMA and LA-ICP-MS investigation on Bi–Cu–Au mineralization from the Kizhnica ore field (Vardar Zone, Kosovo). *Minerals* 11: 1223
- MEDERSKI S, WOJSLAW M, PRŠEK J, MAJZLAN J, KIEFER S, ASLLANI B (2021b) A geochemical study of gersdorffite from the Trepča Mineral Belt, Vardar Zone, Kosovo. *J Geosci* 66: 97–115
- MEDERSKI S, PRŠEK J, DIMITROVA D (2021c) Geochemistry of tetrahedrite group minerals from the Janjevo Cu–Bi–Ag(Pb,W) locality, Kosovo: Results of EPMA and LA-ICP-MS investigations. *Acta Mineral Petrogr* 11: 29
- MEDERSKI S, PRŠEK J, MAJZLAN J, KIEFER S, DIMITROVA D, MILOVSKÝ R, KOCH CB, KOZIEŃ D (2022a) Geochemistry and textural evolution of As–Ti–Sb–Hg-rich pyrite from a sediment-hosted As–Sb–Ti–Pb±Hg±Au mineralization in Janjevo, Kosovo. *Ore Geol Rev* 151: 105221
- MEDERSKI S, PRŠEK J, DIMITROVA D (2022b) Trace elements in sphalerite from the Kizhnica–Hajvalia–Badovc ore field, Kosovo: an example of In-bearing sphalerite. In: *Proceedings of The critical role of minerals in the carbon-neutral future 16th Biennial SGA Meeting*. Rotorua, New Zealand, pp 239–242
- MILÉSI JP, MARCOUX E, NEHLIG P, SUNARYA Y, SUKANDAR A, FELENC J (1994) Cirotan, West Java, Indonesia: a 1.7 Ma hybrid epithermal Au–Ag–Sn–W deposit. *Econ Geol* 89: 227–245
- MOĚLO Y, MAKOVICKY E, MOZGOVA NN, JAMBOR JL, COOK N, PRING A, PAAR W, NICKEL EH, GRAESER S, KARUP-MØLLER S, BALIĆ-ŽUNIĆ T, MUMME WG, VURRO F, TOPA D (2008) Sulfosalt systematics: a review. Report of the sulfosalt sub-committee of the IMA Commission on Ore Mineralogy. *Eur J Mineral* 20: 7–62
- MURAKAMI H, ISHIHARA S (2013) Trace elements of Indium-bearing sphalerite from tin–polymetallic deposits in

- Bolivia, China and Japan: A femto-second LA-ICPMS study. *Ore Geol Rev* 53: 223–243
- RADOSAVLJEVIĆ-MIHAILOVIĆ AS, STOJANOVIĆ JN, DIMITRIJEVIĆ RZ, RADOSAVLJEVIĆ SA (2007) Rare Pb–Bi sulfosalt mineralization from the Boranja ore-field (Podrinje district, Serbia). *Neu Jb Mineral, Abh* 217–224
- RADOSAVLJEVIĆ SA, STOJANOVIĆ JN, RADOSAVLJEVIĆ-MIHAILOVIĆ AS, KAŠIĆ VD (2013) Polymetallic mineralization of the Boranja orefield, Podrinje Metallogenic District, Serbia: zonality, mineral associations and genetic features. *Period Mineral* 82: 61–87
- RADOSAVLJEVIĆ SA, STOJANOVIĆ JN, VUKOVIĆ NS, RADOSAVLJEVIĆ-MIHAILOVIĆ AS, KAŠIĆ VD (2015) Low-temperature Ni–As–Sb–S mineralization of the Pb(Ag)-Zn deposits within the Rogozna ore field, Serbo-Macedonian Metallogenic Province: Ore mineralogy, crystal chemistry and paragenetic relationships. *Ore Geol Rev* 65: 213–227
- SEJKORA J, PAULIŠ P, LITOHLEB J, NOVÁK F (2010) Contribution to chemical composition of the minerals of pearceite-polybasite group from Vrančice near Příbram (Czech Republic). *Bull Mineral Petrolog Odd Nár Muz (Praha)* 18: 23–32 (in Czech)
- SILYANOV SA, SAZONOV AM, NAUMOV EA, LOBASTOV BM, ZVYAGINA YA, ARTEMYEV DA, NEKRASOVA NA, PIRAJNO F (2022) Mineral paragenesis, formation stages and trace elements in sulfides of the Olympiada gold deposit (Yenisei Ridge, Russia). *Ore Geol Rev* 143: 104750
- SIRON CR, THOMPSON JFH, BAKER T, FRIEDMAN R, TSITSANIS P, RUSSELL S, RANDALL S, MORTENSEN J (2016) Magmatic and metallogenic framework of Au–Cu porphyry and polymetallic carbonate-hosted replacement deposits of the Kassandra mining district, Northern Greece. *SEG Spec Publ* 19: 29–55
- SITARZ M, GOŁĘBIEWSKA B, NEJBERT K, DIMITROVA D, MILOVSKÝ R (2021) Hydrothermal ore mineralization from the Polish part of the Tatra Mts., Central Western Carpathians. *Geol Geophys Environ* 47: 159–179
- SKOUPRAS E, MELFOS V, VOUDOURIS P, STERGIU CL, KANTIRANIS N, PAPADOPOULOU L, SAKELLARIS G-A (2022). The stibnite vein-type mineralization in Rizana, Northern Greece. In the Abstract Proceedings of the XXII International Congress of the CBGA, Plovdiv, Bulgaria, 7.–11. September 2022, 200
- SPRINGER G (1971) The synthetic solid-solution series Bi_2S_3 – BiCuPbS_3 (bismuthinite–aikinite). *Neu Jb Mineral, Mh* 19–24
- STOJANOVIĆ J, RADOSAVLJEVIĆ SA, KARANOVIC L, CVETKOVIĆ L (2006) Mineralogy of W–Pb–Bi ores from Rudnik Mt., Serbia. *Neu Jb Mineral, Abh* 182: 299–306
- STOJANOVIĆ JN, RADOSAVLJEVIĆ SA, TOŠOVIĆ RD, PAČEVSKI AM, RADOSAVLJEVIĆ-MIHAILOVIĆ AS, KAŠIĆ VD, VUKOVIĆ NS (2018) A review of the Pb–Zn–Cu–Ag–Bi–W polymetallic ore from the Rudnik orefield, Central Serbia. *Geol An Balkan Poluostr* 79: 47–69
- STRMIĆ PALINKAŠ S, PALINKAŠ LA, RENAC C, SPANGENBERG JE, LÜDERS V, MOLNAR F, MALIQI G (2013) Metallogenic model of the Trepča Pb–Zn–Ag skarn deposit, Kosovo: evidence from fluid inclusions, rare earth elements, and stable isotope data. *Econ Geol* 108: 135–162
- TĂMAȘ CG, ANDRII M-P (2020) Mineralogy of skarn ores from Băița-Bihor, Northern Apuseni Mountains, Romania: A case study of Cu-, Bi-, and Sn-minerals. *Minerals* 10: 436
- TOPA D, MAKOVICKY E (2010) The crystal chemistry of cosalite based on new electron-microprobe data and single-crystal determinations of the structure. *Canad Mineral* 48: 2082–2207
- TOPA D, MAKOVICKY E, PAAR WH (2002) Composition ranges and exsolution pairs for the members of the bismuthinite–aikinite series from Felbertal, Austria. *Canad Mineral* 40: 849–869
- TOPA D, PETŘÍČEK V, DUŠEK M, MAKOVICKY E, BALIĆ-ŽUNIĆ T (2008) Simultaneous refinement of two components of an exsolution intergrowth: Crystal structures of the lindströmite–krupkaite pair. *Canad Mineral* 46: 525–539
- TOPA D, MAKOVICKY E, ILINCA G, DITTRICH H (2012) Cupromakopavonite, $\text{Cu}_8\text{Ag}_3\text{Pb}_4\text{Bi}_{19}\text{S}_{38}$, a new mineral species, its crystal structure and the cupropavonite homologous series. *Canad Mineral* 50: 295–312
- VOUDOURIS P, MELFOS V, SPRY PG, BONSALE TA, TARKIAN M, SOLOMOS CH (2008) Carbonate-replacement Pb–Zn–Ag±Au mineralization in the Kamariza area, Lavrion, Greece: Mineralogy and thermochemical conditions of formation. *Mineral Petrol* 94: 85–106
- VOUDOURIS PC, SPRY PG, MAVROGONATOS C, SAKELLARIS G-A, BRISTOL SK, MELFOS V, FORNADEL AP (2013) Bismuthinite derivatives, lillianite homologues, and bismuth sulfotellurides as indicators of gold mineralization in the Stanos shear-zone related deposit, Chalkidiki, northern Greece. *Canad Mineral* 51: 119–142
- VOUDOURIS P, MAVROGONATOS C, RIECK B, KOLITSCH U, SPRY P, SCHEFFER C, TARANTOLA A, VANDERHAEGHE O, GALANOS E, MELFOS V, ZAIMIS S, SOUKIS K, PHOTIADES A (2018) The gersdorffite–bismuthinite–native gold association and the skarn–porphyry mineralization in the Kamariza mining district, Lavrion, Greece. *Minerals* 8: 531
- VOUDOURIS P, REPSTOCK A, SPRY PG, FRENZEL M, MAVROGONATOS C, KEITH M, TARANTOLA A, MELFOS V, TOMBROS S, ZHAI D, COOK NJ, CIOBANU CL, SCHAARSCHMIDT A, RIECK B, KOLITSCH U, FALKENBERG JJ (2022) Physicochemical constraints on indium-, tin-, germanium-, gallium-, gold-, and tellurium-bearing mineralizations in the Pefka and St Philippos polymetallic vein- and breccia-type deposits, Greece. *Ore Geol Rev* 140: 104348
- WAGNER T, WILLIAMS-JONES AE, BOYCE AJ (2005) Stable isotope-based modeling of the origin and genesis of an

- unusual Au–Ag–Sn–W epithermal system at Cirotan, Indonesia. *Chem Geol* 219: 237–260
- WANG K, ZHAI D, LIU J, WU H (2021) LA-ICP-MS trace element analysis of pyrite from the Dafang gold deposit, South China: Implications for ore genesis. *Ore Geol Rev* 139: 104507
- WĘGRZYNOWICZ J, PRŠEK J, MEDERSKI S, ASLLANI B, KANIGOWSKI J (2019) Pb–Bi(–Cu) and Pb–Sb sulfosalts from Stan Terg area, Kosovo. In: *Proceedings of the Life with Ore Deposits on Earth: 15th Biennial SGA Meeting*. University of Glasgow Publicity Services, Glasgow, Scotland, pp 380–383
- WESTNER K (2017) Roman mining and metal production near the antique city of Ulpiana (Kosovo). PhD Thesis, Goethe-Universität, Frankfurt, pp 1–429
- XU J, COOK NJ, CIOBANU CL, LI X, KONTONIKAS-CHAROS A, GILBERT S, LV Y (2021) Indium distribution in sphalerite from sulfide–oxide–silicate skarn assemblages: a case study of the Dulong Zn–Sn–In deposit, Southwest China. *Miner Depos* 56: 307–324
- YATIMOV UA, AYUPOVA NR, BLINOV IA, KOTLYAROV VA (2019) Bismuth minerals of the sulfide-magnetite ores of the Aktash deposit (Western Karamazar, Tajikistan). *Mineralogiya* 5: 39–51 (in Russian)